Ballistic matter waves with angular momentum: Exact solutions and applications

Christian Bracher,[1,*] Tobias Kramer,[2] and Manfred Kleber[2]
[1]*Department of Physics and Atmospheric Science, Dalhousie University, Halifax, Nova Scotia, Canada B3H 3J5*
[2]*Physik-Department T30c, Technische Universität München, James-Franck-Strasse, 85747 Garching, Germany*
(Received 5 November 2002; published 4 April 2003)

An alternative description of quantum scattering processes rests on inhomogeneous terms amended to the Schrödinger equation. We detail the structure of sources that give rise to multipole scattering waves of definite angular momentum, and introduce pointlike multipole sources as their limiting case. We obtain results for ballistic scattering in an external uniform force field, where we provide analytical solutions for both the scattering waves and the integrated particle flux. Our theory directly applies to *p*-wave photodetachment in an electric field. Furthermore, illustrating the effects of extended sources, we predict some properties of vortex-bearing atom laser beams outcoupled from a rotating Bose-Einstein condensate under the influence of gravity.

DOI: 10.1103/PhysRevA.67.043601 PACS number(s): 03.75.Pp, 03.65.Nk, 03.75.Kk, 32.80.Gc

I. INTRODUCTION

The customary approach to elastic quantum scattering phenomena employs a superposition of an incoming plane wave and an outbound scattering wave that emerges from a localized scattering potential. It is sometimes advisable to reduce the complexity of this process by dividing the scattering event into subsequent ''absorption'' and ''emission'' stages. The evolution of the emerging wave is then considered separately. Obviously, in this description a ''reservoir'' of particles in the interaction region is required that continuously feeds the stationary scattering wave. Since the particle number is a conserved quantity in the standard quantum picture, we devise a modified approach: In analogy to electrodynamics and other field theories, an inhomogeneous ''source term'' added to the Schrödinger equation allows for particle generation in a finite volume. It was Schwinger who introduced the idea of particle sources in field theory in order to avoid the use of operator fields. Interestingly enough, he also presented the nonrelativistic limit of such a particle source [1]. Recent examples illustrating the use of the source formalism are presented in Refs. [2–4].

In our contribution, we inquire into quantum sources that give rise to scattering waves carrying nonvanishing angular momentum, which we will denote as multipole waves. In the long-wave (or low-energy) limit, apart from its angular dependence the actual structure of the source becomes insignificant, and the scattering process may be properly modeled using an idealized pointlike source of suitable orbital symmetry. Technically, these ''multipole sources'' are obtained from the Dirac δ distribution (that itself pertains to isotropic or *s*-wave emission, see Ref. [4]) by a simple differentiation procedure outlined in Sec. II that grants immediate access to the corresponding multipole wave and currents.

For scattering waves propagating freely (or in a central potential), multipole sources generate the spherical waves familiar from partial-wave theory. Nontrivial results emerge, however, when the scattered particles are subject to acceleration in a homogeneous force field [4,5]. We present analytical expressions for the ensuing ballistic multipole waves and currents, and discuss some of their intriguing features in Sec. III. These developments are directly applicable towards near-threshold photodetachment microscopy, an experimental technique recently introduced by Blondel *et al.* [6,7] that allows to observe interference of electron waves on a macroscopic scale. Here, we predict the photoelectron distribution in *p*-wave detachment (Sec. IV).

In general, the multipole formalism breaks down when the spatial extension of the source becomes comparable to the particle wavelength. In the ballistic environment, Gaussian sources provide an important exception since the scattering waves generated by them apparently converge onto a displaced pointlike ''virtual source'' [4]. Actually, this situation is encountered for an atom laser beam outcoupled from an ideal Bose-Einstein condensate (BEC) that is subsequently accelerated in the earth's gravitational field [8,9]. Angular-momentum transfer to the superfluid condensate leads to the formation of vortices that in turn act as sources for higher modes of the resulting atom laser. The effects of vortices on the beam profile are the topic of Sec. V. Exact solutions are presented for a single vortex in an otherwise spherically symmetric ideal BEC. Furthermore, we investigate the structures imprinted on the atomic beam by the rotating vortex lattices recently realized experimentally [10–12].

II. QUANTUM SOURCES

Following a brief overview of the source formalism and its basic results, emphasizing its kinship to conventional scattering theory, this section is mainly concerned with the properties of idealized ''multipole sources'' for particles with definite angular momentum that emerge in the long-wave limit. For freely propagating particles, the connection to the partial-wave formalism is straightforward. For simplicity, here we investigate elastic potential scattering [13]. However, the source approach is readily extended to more sophisticated problems such as the atom laser (Sec. V), as illustrated in Ref. [4].

*Electronic address: cbracher@fizz.phys.dal.ca

A. Currents generated by a quantum source

In the customary treatment of scattering, the total wave function $\psi(\mathbf{r})$ in the potential $V(\mathbf{r})$ is decomposed into an incoming wave $\psi_{\rm in}(\mathbf{r})$, and a scattered wave $\psi_{\rm sc}(\mathbf{r})$ that may be written as a sum of partial waves $\psi_{lm}(\mathbf{r})$ of definite spherical symmetry: $\psi(\mathbf{r})=\psi_{\rm in}(\mathbf{r})+\psi_{\rm sc}(\mathbf{r})$. Obviously, $\psi_{\rm in}(\mathbf{r})$ is not an eigenfunction to the full Hamiltonian $H=T+V$, but rather to a simpler "unperturbed" Hamiltonian $H_0=T+U$: $H_0\psi_{\rm in}(\mathbf{r})=E\psi_{\rm in}(\mathbf{r})$. (Often, one sets $U=0$. When long-range forces are present, like in Coulomb scattering [13], this choice is poor, and $U(\mathbf{r})$ should account for the interaction potential. See also Sec. III.) Consequently, this procedure leads to the introduction of the scattering potential $W(\mathbf{r})=V(\mathbf{r})-U(\mathbf{r})$, and the stationary Schrödinger equation reads, as usual, $[E-H]\psi(\mathbf{r})=0$ or

$$[E-H_0][\psi_{\rm in}(\mathbf{r})+\psi_{\rm sc}(\mathbf{r})]=W(\mathbf{r})[\psi_{\rm in}(\mathbf{r})+\psi_{\rm sc}(\mathbf{r})]. \quad (1)$$

Since $\psi_{\rm in}(\mathbf{r})$ is an eigenfunction to H_0, we may state Eq. (1) in the equivalent form

$$[E-H_0-W(\mathbf{r})]\psi_{\rm sc}(\mathbf{r})=W(\mathbf{r})\psi_{\rm in}(\mathbf{r}). \quad (2)$$

We infer that the scattering wave $\psi_{\rm sc}(\mathbf{r})$ solves a Schrödinger equation for the full Hamiltonian $H=H_0+W(\mathbf{r})$, albeit with an additional inhomogeneous term $\sigma(\mathbf{r})=W(\mathbf{r})\psi_{\rm in}(\mathbf{r})$ present.

In view of other inhomogeneous field equations, e.g., Maxwell's equations, the right-hand term $\sigma(\mathbf{r})$ in Eq. (2) is identified as a source for the scattering wave $\psi_{\rm sc}(\mathbf{r})$. This observation motivates a simple picture for the scattering process: The incoming wave $\psi_{\rm in}(\mathbf{r})$, via the perturbation $W(\mathbf{r})$, feeds particles into the scattering wave $\psi_{\rm sc}(\mathbf{r})$ governed by the Hamiltonian H. Thus, the decomposition of the wave function into an incoming and a scattered part naturally leads to the notion of a quantum source.

We now turn to the mathematical aspects of Eq. (2). Introducing the energy Green function $G(\mathbf{r},\mathbf{r}';E)$ for the Hamiltonian H defined via [14]

$$[E-H_0-W(\mathbf{r})]G(\mathbf{r},\mathbf{r}';E)=\delta(\mathbf{r}-\mathbf{r}'), \quad (3)$$

a solution to Eq. (2) in terms of a convolution integral reads

$$\psi_{\rm sc}(\mathbf{r})=\int d^3r'\,G(\mathbf{r},\mathbf{r}';E)\sigma(\mathbf{r}'). \quad (4)$$

In general, this result is not unique, since any eigenfunction $\psi_{\rm hom}(\mathbf{r})$ of H may be added. The ambiguity in $\psi_{\rm sc}(\mathbf{r})$ is resolved by the demand that $G(\mathbf{r},\mathbf{r}';E)$ presents a retarded solution characterized by outgoing-wave behavior as $r\to\infty$. Formally, this enforces the choice $G=\lim_{\eta\to 0^+}[E-H+i\eta]^{-1}$ which is equivalent to (Ref. [15]):

$$G(\mathbf{r},\mathbf{r}';E)=\left\langle \mathbf{r}\left|\mathrm{P}\left(\frac{1}{E-H}\right)-i\pi\delta(E-H)\right|\mathbf{r}'\right\rangle, \quad (5)$$

where $\mathrm{P}(\cdots)$ denotes the Cauchy principal value of the energy integration.

Defining the current density in the scattering wave in the usual fashion by $\mathbf{j}(\mathbf{r})=\hbar\,\mathrm{Im}[\psi_{\rm sc}(\mathbf{r})^*\boldsymbol{\nabla}\psi_{\rm sc}(\mathbf{r})]/M$ (where for simplicity we omitted the vector potential $\mathbf{A}(\mathbf{r})$, see Ref. [3]), the inhomogeneous Schrödinger equation (2) gives rise to a modified equation of continuity [2,4]:

$$\boldsymbol{\nabla}\cdot\mathbf{j}(\mathbf{r})=-\frac{2}{\hbar}\mathrm{Im}[\sigma(\mathbf{r})^*\psi_{\rm sc}(\mathbf{r})]. \quad (6)$$

Thus, the inhomogeneity $\sigma(\mathbf{r})$ also acts as a source for the particle current $\mathbf{j}(\mathbf{r})$. By integration over the source volume, and inserting Eq. (4), we obtain a bilinear expression for the total particle current $J(E)$, i.e., the total scattering rate

$$J(E)=-\frac{2}{\hbar}\mathrm{Im}\left[\int d^3r\int d^3r'\,\sigma(\mathbf{r})^*G(\mathbf{r},\mathbf{r}';E)\sigma(\mathbf{r}')\right]. \quad (7)$$

Some important identities concerning the total current $J(E)$ are most easily recognized in a formal Dirac bra-ket representation. In view of Eq. (5), we may express $J(E)$ by

$$J(E)=-\frac{2}{\hbar}\mathrm{Im}[\langle\sigma|G|\sigma\rangle]=\frac{2\pi}{\hbar}\langle\sigma|\delta(E-H)|\sigma\rangle, \quad (8)$$

from which the sum rule immediately follows [4]:

$$\int_{-\infty}^{\infty}dE\,J(E)=\frac{2\pi}{\hbar}\langle\sigma|\sigma\rangle=\frac{2\pi}{\hbar}\int d^3r|\sigma(\mathbf{r})|^2, \quad (9)$$

(provided this integral exists). In order to connect Eq. (7) to the findings of conventional scattering theory, we display $J(E)$ in an entirely different, yet wholly equivalent fashion. Employing a complete orthonormal set of eigenfunctions $|\psi_{\rm fi}\rangle$ of the Hamiltonian H, $\delta(E-H)|\psi_{\rm fi}\rangle=\delta(E-E_{\rm fi})|\psi_{\rm fi}\rangle$ follows, and replacing $|\sigma\rangle=W|\psi_{\rm in}\rangle$ (5), we may formally decompose Eq. (8) into a sum over eigenfunctions:

$$J(E)=\frac{2\pi}{\hbar}\sum_{\rm fi}\delta(E-E_{\rm fi})|\langle\psi_{\rm fi}|W|\psi_{\rm in}\rangle|^2. \quad (10)$$

Thus, Fermi's golden rule is recovered. Another noteworthy consequence of Eqs. (7) and (8) emerges in the limit of pointlike sources, $\sigma(\mathbf{r})\sim C\delta(\mathbf{r}-\mathbf{R})$. We then find [2]

$$J(E)=-\frac{2}{\hbar}|C|^2\mathrm{Im}[G(\mathbf{R},\mathbf{R};E)]=\frac{2\pi}{\hbar}|C|^2n(\mathbf{R};E), \quad (11)$$

where $n(\mathbf{R};E)=\Sigma_{\rm fi}\delta(E-E_{\rm fi})|\psi_{\rm fi}(\mathbf{R})|^2$ is the local density of states of H at the source position $\mathbf{R}$. Equation (11) forms the theoretical basis of the Tersoff-Hamann description of scanning tunneling microscopy [2,16].

B. Multipole sources, waves, and currents

The theory of quantum sources becomes particularly simple for pointlike sources, since the otherwise bothersome integrations involved in the determination of the scattering wave $\psi_{\rm sc}(\mathbf{r})$ (4) and the total current $J(E)$ (7) then become

trivial. For the naive choice of a point source, $\sigma(\mathbf{r})=C\delta(\mathbf{r}-\mathbf{R})$, $\psi_{\mathrm{sc}}(\mathbf{r})$ is simply proportional to the Green function $G(\mathbf{r},\mathbf{R};E)$ itself, and $J(E)$ follows from the Tersoff-Hamann rule (11). The approximation of a pointlike source is obviously well justified in near-threshold scattering ($E\to 0$), where the long wavelength of the emerging wave effectively obliterates the internal structure of the source. This statement, however, must be taken *cum grano salis*, for it does not take into account the orbital structure of the scattering wave.

In fact, the point source $\sigma(\mathbf{r})\sim\delta(\mathbf{r}-\mathbf{r}')$ invariably leads to locally isotropic emission, i.e., describes scattering into an *s*-wave. Despite often being appropriate in practice [3,6,7], conservation of angular momentum may enforce selection rules that restrict scattering to higher multipole waves. For these, we must suitably modify the idealized point-source approach. We proceed by analogy with the multipole formalism commonly used in potential theory, the simplest inhomogeneous field equation.

Like the scattering wave for a simple point source, the Green function of potential theory equals the field created by a source of unit strength located at $\mathbf{r}'$, $G(\mathbf{r},\mathbf{r}')=-1/4\pi|\mathbf{r}-\mathbf{r}'|$. Additional solutions that likewise show a singularity at $\mathbf{r}'$ can be constructed via differentiation with respect to the source position $\mathbf{r}'=(x',y',z')$. Of special significance are the multipole potentials $\Phi_{lm}(\mathbf{r},\mathbf{r}')$,

$$\Phi_{lm}(\mathbf{r},\mathbf{r}')=\frac{Y_{lm}(\hat{\boldsymbol{e}}_{\mathbf{r}-\mathbf{r}'})}{|\mathbf{r}-\mathbf{r}'|^{l+1}}=\frac{K_{lm}(\mathbf{r}-\mathbf{r}')}{|\mathbf{r}-\mathbf{r}'|^{2l+1}},\tag{12}$$

as they clearly show (l,m) spherical symmetry. Here, we introduced the harmonic polynomials $K_{lm}(\mathbf{r})=r^lY_{lm}(\hat{r})$, homogeneous polynomials of order l in the coordinates x,y,z that are eigenfunctions of the angular-momentum operator [17–19]. Interestingly, the same polynomial in momentum space, known as the spherical tensor gradient $K_{lm}(\boldsymbol{\nabla}')=K_{lm}(\partial_{x'},\partial_{y'},\partial_{z'})$ [20–22], extracts the multipole potentials from the Green function $G(\mathbf{r},\mathbf{r}')$,

$$K_{lm}(\boldsymbol{\nabla}')G(\mathbf{r},\mathbf{r}')=-\frac{(2l-1)!!}{4\pi}\Phi_{lm}(\mathbf{r},\mathbf{r}').\tag{13}$$

Thus, the spherical tensor gradient imprints the orbital structure onto $G(\mathbf{r},\mathbf{r}')$. Since $\Delta G(\mathbf{r},\mathbf{r}')=\delta(\mathbf{r}-\mathbf{r}')$ holds, we formally obtain from Eq. (13)

$$\Delta\Phi_{lm}(\mathbf{r},\mathbf{r}')=-\frac{4\pi}{(2l-1)!!}K_{lm}(\boldsymbol{\nabla}')\delta(\mathbf{r}-\mathbf{r}').\tag{14}$$

(Note that the differentiation proceeds with respect to $\mathbf{r}'$.) Apart from prefactors, the multipole potentials $\Phi_{lm}(\mathbf{r},\mathbf{r}')$ are thus generated by the spherical tensor gradients of the δ distribution.

Accordingly, for the purpose of the quantum source problem, we define multipole point sources $\delta_{lm}(\mathbf{r}-\mathbf{r}')$ via [20,21]

$$\delta_{lm}(\mathbf{r}-\mathbf{r}')=K_{lm}(\boldsymbol{\nabla}')\delta(\mathbf{r}-\mathbf{r}').\tag{15}$$

Since $K_{lm}(\boldsymbol{\nabla}')$ and the Hamilton operator $H(\mathbf{r},\mathbf{p})$ always commute, the inhomogeneous Schrödinger equation

$$[E-H]G_{lm}(\mathbf{r},\mathbf{r}';E)=\delta_{lm}(\mathbf{r}-\mathbf{r}')\tag{16}$$

is formally solved by the multipole Green functions $G_{lm}(\mathbf{r},\mathbf{r}';E)$ available from $G(\mathbf{r},\mathbf{r}';E)$ by differentiation

$$G_{lm}(\mathbf{r},\mathbf{r}';E)=K_{lm}(\boldsymbol{\nabla}')G(\mathbf{r},\mathbf{r}';E).\tag{17}$$

[We remark in passing that $G(\mathbf{r},\mathbf{r}';E)$ differs from the *s*-wave multipole Green function $G_{00}(\mathbf{r},\mathbf{r}';E)$ only by a factor $\sqrt{4\pi}$.] The multipole point sources $\delta_{lm}(\mathbf{r}-\mathbf{r}')$ (15) and Green functions (17) provide idealized pointlike sources with internal orbital structure.

For illustration, we briefly consider the case of free-particle propagation [$U(\mathbf{r})=0$]. Here, the Green function reduces to an outgoing spherical wave [14]: $G^{(\mathrm{free})}(\mathbf{r},\mathbf{r}';E)=-Me^{ikR}/2\pi\hbar^2R$, where $E=\hbar^2k^2/2M$ and $\mathbf{R}=\mathbf{r}-\mathbf{r}'$. Starting from Eq. (17), a short calculation yields the free-particle multipole Green functions [23],

$$G_{lm}^{(\mathrm{free})}(\mathbf{r},\mathbf{r}';E)=-\frac{Mk^{l+1}}{2\pi\hbar^2}h_l^{(+)}(kR)Y_{lm}(\hat{\mathbf{R}}),\tag{18}$$

where $h_l^{(+)}(u)$ denotes a spherical Hankel function [13]. Evidently, the multipole approach reproduces the partial spherical waves employed in conventional scattering theory. We point out that the multipole waves (18) bear close kinship to the multipole potentials $\Phi_{lm}(\mathbf{r},\mathbf{r}')$ (12). In the vicinity of the source $\mathbf{r}\to\mathbf{r}'$, $G_{lm}^{(\mathrm{free})}(\mathbf{r},\mathbf{r}';E)$ asymptotically behaves like

$$G_{lm}(\mathbf{r},\mathbf{r}';E)\sim-\frac{M}{2\pi\hbar^2}(2l-1)!!\frac{Y_{lm}(\hat{\boldsymbol{e}}_{\mathbf{r}-\mathbf{r}'})}{|\mathbf{r}-\mathbf{r}'|^{l+1}}.\tag{19}$$

Indeed, it can be shown that Eq. (19) is a universal property of multipole Green functions, provided only that the external potential $U(\mathbf{r})$ is analytic at the source location $\mathbf{r}'$ [23]: Even in a symmetry-breaking environment, the desired (l,m) orbital symmetry locally prevails.

Next, we turn our attention to the currents generated by multipole point sources. Assuming a superposition of several of these sources at a fixed location $\mathbf{r}'$, $\sigma(\mathbf{r})=\Sigma_{lm}\lambda_{lm}\delta_{lm}(\mathbf{r}-\mathbf{r}')$, the resulting scattering wave reads

$$\psi_{\mathrm{sc}}(\mathbf{r})=\sum_{lm}\lambda_{lm}G_{lm}(\mathbf{r},\mathbf{r}';E).\tag{20}$$

The current density $\mathbf{j}(\mathbf{r})$ due to this wave function may be expressed as a bilinear form in the amplitudes λ_{lm}:

$$\mathbf{j}(\mathbf{r})=\sum_{lm}\sum_{l'm'}\lambda_{lm}^*\mathbf{j}_{lm,l'm'}(\mathbf{r})\lambda_{l'm'},\tag{21}$$

where the (vector) elements of the Hermitian current-density matrix $\mathbf{j}_{lm,l'm'}(\mathbf{r})$ are given by

$$\mathbf{j}_{lm,l'm'}(\mathbf{r}) = -\frac{i\hbar}{2M}\{G^*_{lm}(\mathbf{r},\mathbf{r}';E)\boldsymbol{\nabla} G_{l'm'}(\mathbf{r},\mathbf{r}';E) - G_{l'm'}(\mathbf{r},\mathbf{r}';E)\boldsymbol{\nabla} G^*_{lm}(\mathbf{r},\mathbf{r}';E)\}. \quad (22)$$

Of particular interest is the total current $J(E)$ carried by the scattering wave (20), i.e., the integrated current density $\mathbf{j}(\mathbf{r})$ (21). It is available from Eq. (7) through integration by parts. A slight rearrangement yields again a bilinear expression for $J(E)$,

$$J(E) = \sum_{lm}\sum_{l'm'} \lambda^*_{lm} J_{lm,l'm'}(E)\lambda_{l'm'}. \quad (23)$$

The components of the Hermitian total multipole current matrix $J_{lm,l'm'}(E)$ can be extracted from the Green function $G(\mathbf{r},\mathbf{r}';E)$ through differentiation operations and a subsequent limiting procedure:

$$J_{lm,l'm'}(E) = \frac{i}{\hbar}\lim_{\mathbf{r}\to\mathbf{r}'} K^*_{lm}(\boldsymbol{\nabla})K_{l'm'}(\boldsymbol{\nabla}')\{G(\mathbf{r},\mathbf{r}';E) - G(\mathbf{r}',\mathbf{r};E)^*\}. \quad (24)$$

For simplicity, we will denote the (real and positive) diagonal elements of this matrix as the (l,m) multipole currents $J_{lm}(E)$: $J_{lm}(E) = J_{lm,lm}(E)$. For free propagation, these currents are readily evaluated [23]:

$$J^{(\mathrm{free})}_{lm}(E) = \frac{M}{4\pi^2\hbar^3}k^{2l+1}. \quad (25)$$

The characteristic power-law dependence of the scattering rate near the threshold is known as Wigner's law [24].

In the case $U(\mathbf{r}) = 0$, all off-diagonal elements $J^{(\mathrm{free})}_{lm,l'm'}(E)$ are zero, and the total current in Eq. (23) becomes a simple sum $J^{(\mathrm{free})}(E) = \Sigma_{lm}|\lambda_{lm}|^2 J^{(\mathrm{free})}_{lm}(E)$. This is due to the angular symmetry of the Hamiltonian H: Assume that the generator of a rotation L commutes with H; then, it will also commute with the resolvent operator $G = [E - H + i\eta]^{-1}$. Consequently, if the source states $|\sigma\rangle$ and $|\sigma'\rangle$ are eigenstates of L with different eigenvalues, the mixed matrix element $\langle\sigma|G|\sigma'\rangle$, and hence its contribution to the total current $J(E)$ in Eq. (8), is bound to vanish. If the potential $U(\mathbf{r})$ is invariant merely with respect to rotations around the z axis (such as in the ballistic problem discussed in detail in Sec. III), orthogonality with respect to different values of m prevails: $J_{lm,l'm'}(E) = 0$ for $m \neq m'$.

Finally, we set out to extend the Tersoff-Hamann description (11) of the current to cover the case of multipole point sources. According to Eq. (7), the current $J_{lm}(E)$ for a source located at $\mathbf{R}$ is formally given by $J_{lm}(E) = 2\pi\langle\mathbf{R}|K^*_{lm}(\mathbf{p})\,\delta(E-H)K_{lm}(\mathbf{p})|\mathbf{R}\rangle/\hbar$. Expanding this expression again into a complete orthonormal set of eigenfunctions $|\psi_{\mathrm{fi}}\rangle$ of H, we find

$$J_{lm}(E) = \frac{2\pi}{\hbar}\sum_{\mathrm{fi}} \delta(E - E_{\mathrm{fi}})|K_{lm}(\boldsymbol{\nabla})\psi_{\mathrm{fi}}(\mathbf{R})|^2. \quad (26)$$

Therefore, the multipole currents $J_{lm}(E)$ (26) are proportional to the local density of the respective spherical tensor gradients of the eigenstates of the Hamiltonian H at energy E and position $\mathbf{R}$.

III. BALLISTIC MULTIPOLE WAVES AND CURRENTS

So far, we applied the multipole wave approach to freely propagating particles, where it merely reproduces the well-known results of partial-wave decomposition [13]. In this section, we will tackle a less trivial problem, the propagation of a multipole scattering wave accelerated by a homogeneous force field $\mathbf{F} = F\hat{\boldsymbol{e}}_z$, i.e., in the presence of a linear potential $U(\mathbf{r}) = -Fz$. (Subsequently, we will refer to the dynamics in this environment as quantum ballistic motion.) As an analytical expression for the corresponding Green function $G(\mathbf{r},\mathbf{r}';E)$ (3) is available, the developments of Sec. II B allow us to present the solution to the ballistic multipole problem in closed form. Applications of the theory to physical phenomena under current study are presented in Secs. IV and V.

A. The ballistic Green function

As an extension of the method of Green functions $G(\mathbf{r},\mathbf{r}';E)$, the multipole source approach requires knowledge of the latter for a given background potential $U(\mathbf{r})$. However, only for a scarce number of realistic, three-dimensional potentials the Green function is known in closed form. Besides free propagation, this selection comprises the Coulomb potential $U(\mathbf{r}) = \alpha/|\mathbf{r}-\mathbf{R}|$ [25,26], the isotropic harmonic oscillator [27], the homogeneous magnetic field [28,29], and parallel electric and magnetic fields [3,30]. For the ballistic problem, an analytic expression for the Green function was derived independently by several authors [31–33]:

$$G(\mathbf{r},\mathbf{r}';E) = \frac{M}{2\hbar^2}\frac{1}{|\mathbf{r}-\mathbf{r}'|}[\mathrm{Ci}(\alpha_+)\mathrm{Ai}'(\alpha_-) - \mathrm{Ci}'(\alpha_+)\mathrm{Ai}(\alpha_-)], \quad (27)$$

where the arguments $\alpha_\pm$ of the Airy functions $\mathrm{Ai}(u)$, $\mathrm{Ci}(u) = \mathrm{Bi}(u) + i\,\mathrm{Ai}(u)$ [34] are given by

$$\alpha_\pm = -\beta[2E + F(z+z') \pm F|\mathbf{r}-\mathbf{r}'|]. \quad (28)$$

(A rather elementary derivation of this result is presented in Ref. [5].) Here, β denotes an inverse energy scale of the system that varies with the force strength F:

$$\beta = (M/4\hbar^2F^2)^{1/3}. \quad (29)$$

It is convenient to introduce dimensionless quantities for the energy, time, position, and momentum variables,

$$\boldsymbol{\rho} = \beta F\mathbf{r}, \quad \epsilon = -2\beta E, \quad \boldsymbol{\kappa} = \mathbf{k}/\beta F, \quad \tau = t/2\hbar\beta. \quad (30)$$

[The components of $\boldsymbol{\rho}$ will be denoted by $\boldsymbol{\rho}=(\xi,\upsilon,\zeta)^T$.] We state two helpful integral representations of the Green function (27) in this notation. The first follows from a Laplace transform of the time-dependent ballistic propagator $K(\mathbf{r},t|\mathbf{r}',t')$ [4]:

$$G(\boldsymbol{\rho},\boldsymbol{\rho}';\epsilon)=-2i\beta(\beta F)^3\int_0^\infty \frac{d\tau}{(i\pi\tau)^{3/2}} \times e^{i[(\boldsymbol{\rho}-\boldsymbol{\rho}')^2/\tau]+i\tau(\zeta+\zeta'-\epsilon)-i\tau^3/12}, \tag{31}$$

while the second form features the propagator in momentum space:

$$G(\boldsymbol{\rho},\boldsymbol{\rho}';\epsilon)=-\frac{i\beta(\beta F)^3}{4\pi^3}\int_0^\infty d\tau e^{-i\epsilon\tau-i\tau^3/12}\int d^3\kappa\int d^3\kappa' \times e^{-i(\boldsymbol{\kappa}\cdot\boldsymbol{\rho}+\boldsymbol{\kappa}'\cdot\boldsymbol{\rho}')-i(\boldsymbol{\kappa}-\boldsymbol{\kappa}')^2/16}\delta(\boldsymbol{\kappa}+\boldsymbol{\kappa}'+2\tau\hat{\boldsymbol{e}}_z). \tag{32}$$

Finally, we point out a useful internal symmetry of the ballistic problem. From Eqs. (27) and (28), we infer that $G(\mathbf{r},\mathbf{r}';E)$ is a functional of the variables $\mathbf{r}-\mathbf{r}'$ and $E+Fz'$ only. This combined translational symmetry results from the uniformity of the force field, where a shift of the source position merely alters the potential energy of the emitted particles. We may take advantage of this invariance to relocate the source to the origin [4]:

$$G(\mathbf{r},\mathbf{r}';E)=G(\mathbf{r}-\mathbf{r}',\mathbf{0};E+Fz'). \tag{33}$$

Furthermore, the exclusive dependence on these variables allows us to replace derivatives of $G(\mathbf{r},\mathbf{r}';E)$ with respect to the source location $\mathbf{r}'$ by derivatives with respect to $\mathbf{r}$ and the energy E. One easily verifies that

$$\boldsymbol{\nabla}' G(\boldsymbol{\rho},\boldsymbol{\rho}';\epsilon)=-\left(\frac{\partial}{\partial\xi},\frac{\partial}{\partial\upsilon},\frac{\partial}{\partial\zeta}+2\frac{\partial}{\partial\epsilon}\right)^T G(\boldsymbol{\rho},\boldsymbol{\rho}';\epsilon). \tag{34}$$

We will summarizingly refer to the exchange of derivatives in Eq. (34) as the substitution rule for the ballistic Green function.

B. Multipole Green functions

We now characterize the multipole Green functions $G_{lm}(\mathbf{r},\mathbf{r}';E)$ (17) of the ballistic problem. In view of the translational symmetry (33), we remark in advance that it suffices to discuss the case $\mathbf{r}'\to\mathbf{0}$; the general expression for $G_{lm}(\mathbf{r},\mathbf{r}';E)$ then follows by properly adjusting the positions $\mathbf{r}$, $\mathbf{r}'$, and the particle energy E.

By definition (17), the multipole Green function is the spherical tensor gradient $K_{lm}(\boldsymbol{\nabla}')$ of the ballistic Green function $G(\mathbf{r},\mathbf{r}';E)$ (27). Since this differential operator reduces to a polynomial in momentum space, it is advantageous to employ the integral representation (32) in performing the differentiation. In the limit $\mathbf{r}'\to\mathbf{0}$, this procedure yields after a suitable shift in the remaining momentum integration variable $\mathbf{q}=\boldsymbol{\kappa}+\tau\hat{\boldsymbol{e}}_z+2\boldsymbol{\rho}/\tau$:

$$G_{lm}(\boldsymbol{\rho},\mathbf{0};E)=\frac{\beta(i\beta F)^{l+3}}{4\pi^3}\int_0^\infty d\tau e^{i(\rho^2/\tau)-i(\epsilon-\zeta)\tau-i\tau^3/12} \times\int d^3q K_{lm}(\mathbf{q}+\tau\hat{\boldsymbol{e}}_z-2\boldsymbol{\rho}/\tau)e^{-i\tau q^2/4}. \tag{35}$$

The latter integral involves the product of a Gaussian with a polynomial expression and hence allows for evaluation in closed form. To this end, we first expand the shifted harmonic polynomial $K_{lm}(\mathbf{q}+\tau\hat{\boldsymbol{e}}_z-2\boldsymbol{\rho}/\tau)$ into a spherical series with respect to $\mathbf{q}$, as demonstrated in Appendix A. Since the Gaussian part is isotropic, the only contribution to the integral stems from the term with $\lambda=\mu=0$ in the series (A1), rendering the calculation trivial. Furthermore, by a repeated application of the translation theorem for harmonic polynomials (A3), we may separate the spatial and temporal dependence in the argument of the remaining function $K_{lm}(\tau\hat{\boldsymbol{e}}_z-2\boldsymbol{\rho}/\tau)$. We then finally obtain a spherical series in $\boldsymbol{\rho}$ for the momentum integral in Eq. (35):

$$\int d^3q K_{lm}(\mathbf{q}+\tau\hat{\boldsymbol{e}}_z-2\boldsymbol{\rho}/\tau)e^{-i\tau q^2/4} =\frac{8\pi^{3/2}}{(i\tau)^{3/2}}(-i)^l\sum_{j=|m|}^{l}2^j T_{jlm}(i\tau)^{l-2j}K_{jm}(\boldsymbol{\rho}), \tag{36}$$

where the translation coefficients T_{jlm} are given by Eq. (A4). At this point, it proves convenient to introduce a set of auxiliary functions $Q_k(\rho,\zeta;\epsilon)$ via

$$Q_k(\rho,\zeta;\epsilon)=\frac{i}{2\pi\sqrt{\pi}}\int_0^\infty\frac{d\tau}{(i\tau)^{k+1/2}} \times\exp\left\{i\left[\frac{\rho^2}{\tau}+\tau(\zeta-\epsilon)-\frac{\tau^3}{12}\right]\right\}. \tag{37}$$

Despite their rather involved appearance, for integer k these integrals can be systematically evaluated in closed form, yielding sums over products of Airy functions, as detailed in Appendix B 1. [Incidentally, apart from a constant prefactor, the function $Q_k(\rho,\zeta;\epsilon)$ equals the ballistic Green function in $2k+1$ spatial dimensions [5]. E.g., a comparison with Eq. (31) reveals that $G(\boldsymbol{\rho},\mathbf{0};\epsilon)=-4\beta(\beta F)^3Q_1(\rho,\zeta;\epsilon)$.] From Eqs. (35)–(37), we then infer that the ballistic multipole Green function $G_{lm}(\mathbf{r},\mathbf{0};E)$ in the original coordinates is given by

$$G_{lm}(\mathbf{r},\mathbf{0};E)=-4\beta(\beta F)^{l+3}\sum_{j=|m|}^{l}(2\beta F)^j T_{jlm}K_{jm}(\mathbf{r}) \times Q_{2j-l+1}(\beta Fr,\beta Fz;-2\beta E). \tag{38}$$

The explicit expressions obtained from Eq. (38) quickly become cumbersome with increasing multipole order l. While the s-wave function $G_{00}(\mathbf{r},\mathbf{o};E)=G(\mathbf{r},\mathbf{o};E)/\sqrt{4\pi}$ is displayed already in Eq. (27), here we merely state formulas for the p waves in ballistic scattering [23]:

$$G_{10}(\mathbf{r},\mathbf{o};E)=\sqrt{\frac{3}{\pi}}\frac{\beta^3F^2}{r^3}\{z[\mathrm{Ci}(\alpha_+)\mathrm{Ai}'(\alpha_-) - \mathrm{Ci}'(\alpha_+)\mathrm{Ai}(\alpha_-)]+2\beta Fr[\beta[z(2E+Fz) - Fr^2]\mathrm{Ci}(\alpha_+)\mathrm{Ai}(\alpha_-)+z\mathrm{Ci}'(\alpha_+)\mathrm{Ai}'(\alpha_-)]\}, \tag{39}$$

$$G_{1,\pm1}(\mathbf{r},\mathbf{o};E)=\sqrt{\frac{3}{2\pi}}\beta^3F^2\frac{x\pm iy}{r^3}\{\mathrm{Ci}'(\alpha_+)\mathrm{Ai}(\alpha_-) - \mathrm{Ci}(\alpha_+)\mathrm{Ai}'(\alpha_-)-2\beta Fr \times[\mathrm{Ci}'(\alpha_+)\mathrm{Ai}'(\alpha_-) + \beta[2E+Fz]\mathrm{Ci}(\alpha_+)\mathrm{Ai}(\alpha_-)]\}. \tag{40}$$

[The arguments $\alpha_\pm$ of the Airy functions have been defined in Eq. (28).] The expressions for higher multipole order are, however, quickly calculated by means of Eq. (38).

Despite being exact for all values of the parameters, the complicated structure of the explicit solutions (38) to the ballistic multipole problem limits their practical use. Fortunately, comparatively simple asymptotic approximations for the vicinity of the source as well as for the far-field limit are available. In the case $\boldsymbol{\rho}\to\mathbf{o}$, we may invoke the asymptotic form of $Q_k(\rho,\zeta;\epsilon)$, Eq. (B6) together with Eq. (A4), to show that $G_{lm}(\mathbf{r},\mathbf{o};E)$ indeed conforms to the universally valid local behavior of multipole Green functions displayed in Eq. (19).

The presence of the uniform force field $\mathbf{F}$ breaks the orbital symmetry of the multipole waves (38) in the far-field region $z\to\infty$. While the invariance for rotations around the z axis is retained, and the Green functions $G_{lm}(\mathbf{r},\mathbf{o};E)$ are eigenfunctions of L_z, the external potential bends the scattering waves in the direction of force, where they form a particle beam centered around the z axis that continues to spread in the lateral directions, while its density profile settles into an invariant shape that reflects the orbital structure of the source. (Images of the spatial emission pattern are depicted in Sec. IV.) We are thus interested in the asymptotic behavior of Eq. (38) in the vicinity of the z axis, i.e., in the limit $\alpha_+\to-\infty$ (28), while α_- remains finite. Its systematic evaluation by a saddle-point technique is covered in Ref. [23] and will not be repeated here; we merely cite its rather simple result

$$G_{lm}(\mathbf{r},\mathbf{o};E)\sim-\frac{\beta}{2}(2i\beta F)^{l+3}\frac{\mathrm{Ci}(\alpha_+)}{\sqrt{-\alpha_+}}(-1)^mZ_{lm}(\alpha_-) \tag{41}$$

that involves again a harmonic polynomial operator through $Z_{lm}(\alpha_-)$,

$$Z_{lm}(\alpha_-)=K_{lm}\left(\frac{\beta Fx}{\sqrt{-\alpha_+}},\frac{\beta Fy}{\sqrt{-\alpha_+}},i\frac{\partial}{\partial\alpha_-}\right)\mathrm{Ai}(\alpha_-). \tag{42}$$

Note that all multipole waves share a common propagating factor, whereas the asymptotic beam profile is contained in the derivative $Z_{lm}(\alpha_-)$. Explicit expressions for s and p waves are tabulated in Sec. IV B.

C. The ballistic multipole current density

In a second step, we continue our analysis of ballistic scattering with the associated current-density distribution $\mathbf{j}(\mathbf{r})$ (21). We find this quantity from $G_{lm}(\mathbf{r},\mathbf{o};E)$ (38) through differentiation, and the calculation of the exact matrix elements $\mathbf{j}_{lm,l'm'}(\mathbf{r},\mathbf{o};E)$ is tedious yet straightforward. (A formula for the s-wave component $j^{(z)}_{00,00}(\mathbf{r},\mathbf{o};E)$ is stated in Ref. [4].) Here, we confine our attention to the current-density profile in the asymptotic sector $z\to\infty$ that has been recorded experimentally [6,7]. In this limit, the current distribution $j^{(z)}(\mathbf{r})\sim\rho(\mathbf{r})v(z)$ is proportional to the probability density $\rho(\mathbf{r})=|\psi_{\mathrm{sc}}(\mathbf{r})|^2$ in the scattering wave, where $v(z)=\sqrt{2Fz/M}$ is the classical velocity of the accelerated particles. Using Eqs. (41) and (42), we find the far-field current distribution, valid for $\alpha_+\to-\infty$, while α_- (28) is bound:

$$j^{(z)}_{lm,l'm'}(\mathbf{r},\mathbf{o};E)\sim-\frac{\beta(2\beta F)^{l+l'+5}}{4\pi\hbar\alpha_+}i^{l'-l}(-1)^{m+m'} \times Z_{lm}(\alpha_-)^*Z_{l'm'}(\alpha_-). \tag{43}$$

The resulting expressions for $l=0,1$ are employed in Sec. IV B. Several semiclassical approximations to this result have appeared in the literature [6,35–38], generally based on the Hamilton-Jacobi theory of uniformly accelerated motion [5]. Here, we briefly examine the current-density profile on a detector screen placed at large distance $z\to\infty$ as a function of the lateral deviation $R=\sqrt{r^2-z^2}$. For $E>0$, within the range of classically allowed motion $\alpha_-<0$, a circular disk of asymptotic radius $R^2_{\mathrm{cl}}=4Ez/F$, particles of energy E may travel along two different parabolic trajectories from the source $\mathbf{r}'=\mathbf{o}$ to their end point $\mathbf{r}$: Classical paths leaving the source under opposite angles (θ,ϕ), $(\pi-\theta,\phi)$ will asymptotically share the same destination $(R=R_{\mathrm{cl}}\sin\theta,\phi)$ on the screen. Thus, the uniform force field maps the orbital characteristics of the multipole source onto an enlarged density distribution at the detector (see Fig. 1).

As in the traditional double-slit setup [39,40], the presence of two alternative classical paths in the uniform force field environment causes interference between the corresponding particle waves and imposes a circular fringe pattern in the current profile first recorded experimentally by Blondel *et al.* [6,7]. Its details depend on the quantum phases $\sigma_\pm(R,\phi;E)$ accumulated along the trajectories $(+)$ and $(-)$. Three different terms contribute to $\sigma_\pm(R,\phi;E)$ (Fig. 1): First, the trajectories will ''inherit'' atomic phases $\gamma(\theta,\phi)$, $\gamma(\pi-\theta,\phi)$ reflecting the orbital structure of the point source; second, particles traveling along the classical

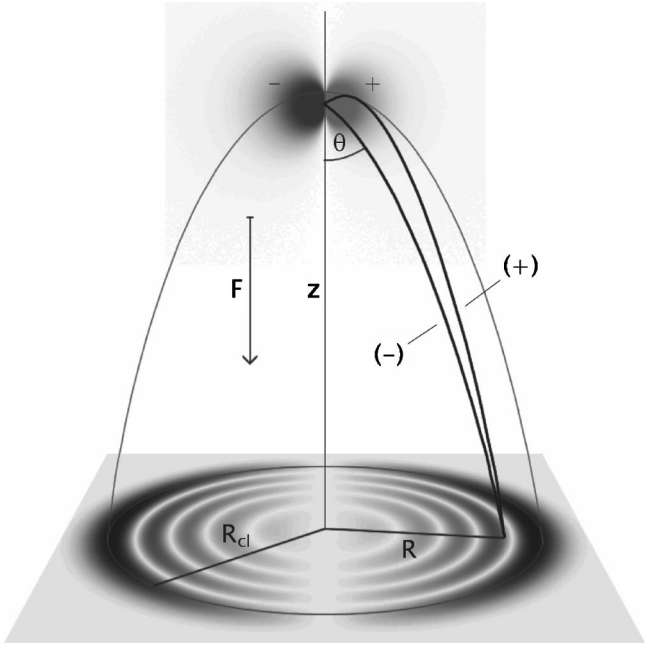

FIG. 1. Semiclassical ballistic motion in the far-field limit. Within the disk $R<R_{\rm cl}$, the two parabolic paths (bold) emitted under opposite angles θ, $\pi-\theta$ will join the point source with the destination. Unlike the fast path $(-)$, the slow path $(+)$ undergoes a reflection at the parabolic turning surface $\alpha_-=0$. The accumulated phases, together with their initial ''atomic'' phases inherited from the source, determine the exact shape of the interference pattern on the screen.

paths will gather dynamical phases which semiclassically are determined by the respective reduced actions $W_{\rm cl}^{(\pm)}(\mathbf{r},\mathbf{0};E)=2\hbar[(-\alpha_+)^{3/2}\pm(-\alpha_-)^{3/2}]/3$ [5]; and finally, the ''slow'' trajectory $(+)$ undergoes an additional ''phase jump'' of $-\pi/2$ due to reflection at the turning surface $\alpha_-=0$ [41]. Denoting the angular amplitude distribution at the source by $A(\theta,\phi)=|A(\theta,\phi)|\exp[i\gamma(\theta,\phi)]$, the semiclassical current-density distribution $j_z^{(\rm sc)}(R,\phi;E)$ on the screen is given by the classical differential cross section $\partial\sigma_{\rm cl}/\partial\Omega(R;E)=R_{\rm cl}^2\cos\theta$, accounting for the projection properties of the force field, modulated by an oscillating term representing the combined effects of orbital source structure and dynamical phase ($\sin\theta=R/R_{\rm cl}$):

$$j_z^{(\rm sc)}(R,\phi;E)=\frac{\partial\Omega}{\partial\sigma_{\rm cl}}(R;E)\big||A(\theta,\phi)|e^{i\sigma_-(R,\phi;E)}+|A(\pi-\theta,\phi)|e^{i\sigma_+(R,\phi;E)}\big|^2. \tag{44}$$

For $|A(\pi-\theta,\phi)|=|A(\theta,\phi)|$, i.e., reflection symmetry of the emission rate with regard to the x-y plane [36], a sharp interference pattern emerges. This condition is always met by pure multipole sources $\delta_{lm}(\mathbf{r})$ (15). In the semiclassical approximation (44), the multipole current $j_{lm,lm}^{(z)}(\mathbf{r},\mathbf{0};E)$ (43) for $z\to\infty$ reads accordingly [23],

$$j_{lm,lm}^{(\rm sc)}(\mathbf{r},\mathbf{0};E)=\frac{Mk^{2l+1}}{4\pi^3\hbar^3}\frac{2l+1}{R_{\rm cl}\sqrt{R_{\rm cl}^2-R^2}}\frac{(l-m)!}{(l+m)!}\times P_l^m\left(\sqrt{1-\frac{R^2}{R_{\rm cl}^2}}\right)^2\times\sin\left\{\frac{2}{3}\left[2\beta E\left(1-\frac{R^2}{R_{\rm cl}^2}\right)\right]^{3/2}\pm\frac{\pi}{4}\right\}^2. \tag{45}$$

Here, $P_l^m(z)$ denotes the associated Legendre polynomial [34], and the upper sign in the interference term applies for even parity, i.e., for even $l-|m|$, whereas the lower sign is valid for odd $l-|m|$. Under change of parity, the circular interference ring pattern will reverse.

We now turn to the case of ballistic tunneling ($E<0$) that is of considerable theoretical interest, being a rare example of a tunneling process in three spatial dimensions yielding to an analytic solution. For the sake of brevity, however, we omit a systematic study here [23]. Rather, we adopt a simple heuristic approach that might be dubbed ''analytic continuation.'' (The case of s-wave ballistic tunneling has been examined in Ref. [5].) We formally take over the former result of Eq. (45) valid for $E>0$, and replace the negative ''classical radius'' $R_{\rm cl}^2$ by its absolute value $R_{\rm tun}^2=4|E|z/F$; quantities derived from it change accordingly, and the geometrical interpretation is lost. Moreover, the tunneling action functional, and hence the phase along the ''trajectories,'' becomes complex [5]. Since the wave function must decay exponentially, the dynamical phase $\sigma(R,\phi;E)$ is uniquely specified in the tunneling regime, and interference is absent. For a pure multipole source $\delta_{lm}(\mathbf{r})$ (15), we finally obtain with the evanescent momentum $\hbar\kappa=\sqrt{2M|E|}$:

$$j_{lm,lm}^{(\rm tun)}(\mathbf{r},\mathbf{0};E)=\frac{M\kappa^{2l+1}}{16\pi^3\hbar^3}\frac{2l+1}{R_{\rm tun}\sqrt{R_{\rm tun}^2+R^2}}\frac{(l-m)!}{(l+m)!}\times\left|P_l^m\left(\sqrt{1+\frac{R^2}{R_{\rm tun}^2}}\right)\right|^2\times\exp\left\{-\frac{4}{3}\left[-2\beta E\left(1+\frac{R^2}{R_{\rm tun}^2}\right)\right]^{3/2}\right\}. \tag{46}$$

[Unlike the Legendre polynomial $P_l^m(z)$ itself, its modulus $|P_l^m(z)|^2$ remains single valued for real $z>1$.]

It is instructive to examine the paraxial limit $R\to0$ of Eq. (46). This yields the following approximation to $j_{lm,lm}^{(\rm tun)}(\mathbf{r},\mathbf{0};E)$, valid for small lateral distances R [5]:

$$j_{lm,lm}^{(\rm tun)}(\mathbf{r},\mathbf{0};E)\sim\frac{M\kappa^{2l+1}}{16\pi^3\hbar^3}\frac{(2l+1)(l+|m|)!}{2^{2|m|}(|m|!)^2(l-|m|)!}\frac{R^{2|m|}}{R_{\rm tun}^{2|m|+2}}\times\exp\left(-\frac{\kappa R^2}{2z}-\frac{\kappa^3}{6(\beta F)^3}\right). \tag{47}$$

For a simple interpretation, we note that the exponential term $\exp[-\kappa^3/6(\beta F)^3]$ equals the WKB penetration factor for a one-dimensional linear potential ramp, while the prefactor $(R/R_{\mathrm{tun}})^{2|m|}$ covers the effect of centrifugal repulsion. It is worth noting that the tunneling current distribution possesses approximately Gaussian form, $J_z^{\mathrm{tun}}(R,\phi;E)\propto\exp(-\kappa R^2/2z)$: Remarkably, the shape of the lateral current profile is largely independent of the force strength F. This prediction is experimentally confirmed in field emission from ultrasharp tips [42].

D. Total ballistic multipole currents

Finally, we derive the total current $J(E)$ (23) carried by a ballistic scattering wave. Its matrix elements $J_{lm,l'm'}(E)$ (24) follow from the Green function $G(\mathbf{r},\mathbf{r}';E)$ (27) by differentiation and a subsequent limiting process, as discussed in Sec. II B. Ahead, we note that due to the rotational symmetry of the force field, the total current matrix is diagonal with respect to the quantum number m, $J_{lm,l'm'}(E)=0$ for $m\neq m'$.

As the multipole formalism invokes spherical tensor gradients $K_{lm}(\boldsymbol{\nabla})$ (24), it is again favorable to use the momentum-space representation of the ballistic Green function $G(\mathbf{r},\mathbf{r}';E)$ (32) in the actual calculation. Then, the differentiation and limit operation are trivial, and the matrix elements of the total current read in integral form

$$J_{lm,l'm'}(E)=\frac{\beta(\beta F)^{l+l'+3}}{2\pi^3\hbar}\mathrm{Im}\Bigg[i^{l-l'+1}\int_0^\infty d\tau e^{-i\epsilon\tau-i\tau^3/12}\times\int d^3q K_{lm}(\mathbf{q}-\tau\hat{\boldsymbol{e}}_z)^*\times K_{l'm'}(\mathbf{q}+\tau\hat{\boldsymbol{e}}_z)e^{-i\tau q^2/4}\Bigg]. \tag{48}$$

Next, the momentum and temporal contributions in the arguments of the harmonic polynomials appearing here are disentangled by means of the translation theorem (A3) (see Appendix A). This renders the angular integration in Eq. (48) straightforward, and the remaining momentum integral is of Gaussian type, leaving only the temporal integral to be evaluated. We may display it as a sum over the auxiliary functions $\mathrm{Qi}_k(\epsilon)=\lim_{\rho,\zeta\to 0}\mathrm{Im}[Q_k(\rho,\zeta;\epsilon)]$ closely related to the expression (37) introduced in Sec. III B:

$$\mathrm{Qi}_k(\epsilon)=\mathrm{Im}\left[\frac{i}{2\pi\sqrt{\pi}}\int_0^\infty\frac{d\tau}{(i\tau)^{k+1/2}}e^{-i\epsilon\tau-i\tau^3/12}\right]. \tag{49}$$

(A similar set of functions is discussed in Ref. [43].) Their properties, in particular, their resolution into products of Airy functions, are discussed in Appendix B 2. With the definition (49), the total ballistic multipole currents $J_{lm,l'm'}(E)$ (24) finally read

$$J_{lm,l'm'}(E)=\delta_{mm'}\frac{M}{2\pi\hbar^3}(\beta F)^{l+l'+1}(-1)^{l+l'}\times\sum_{j=|m|}^{\min(l,l')}2^j(2j+1)!!T_{jlm}T_{jl'm}\times\mathrm{Qi}_{3j-l-l'+1}(-2\beta E). \tag{50}$$

For $l=0,1$, these currents are listed in Sec. IV C.

It is instructive to examine the behavior of the currents $J_{lm}(E)$ for large values of the energy parameter $\epsilon=-2\beta E$. (We treat diagonal matrix elements only.) We have to distinguish between two mathematically and physically rather different cases. First, we consider the limit $\epsilon\gg 1$, i.e., large negative energies. This corresponds to ballistic tunneling from a point source, a phenomenon without classical counterpart. Using the asymptotic series for the auxiliary function $\mathrm{Qi}_k(\epsilon)$ (B12), the total multipole current $J_{lm}(E)$ reads

$$J_{lm}(E)\sim\frac{M\kappa^{2l+1}}{4\pi^2\hbar^3}\frac{(2l+1)(l+|m|)!}{|m|!(l-|m|)!}\left(\frac{\beta F}{\kappa}\right)^{3|m|+3}\times\exp\left(-\frac{\kappa^3}{6(\beta F)^3}\right). \tag{51}$$

Here, $\kappa=2\beta F\sqrt{\epsilon}$ denotes the evanescent particle momentum at the source. As expected, the emission rate drops exponentially with ϵ. We also note that for fixed l, the current strength declines with increasing quantum number $|m|$. This is evidence for the centrifugal suppression of tunneling (see above).

In the classical limit of ballistic motion, $k\to\infty$ (where $k=2\beta F\sqrt{-\epsilon}$, $\epsilon\ll -1$), two terms contribute to the multipole current $J_{lm}(E)$ (see Appendix B 2): The dominant secular term is independent of the field strength F and just reproduces the total current for freely propagating partial waves given by Wigner's law (25). The free-particle expression is modified by an oscillating contribution akin to Eq. (51):

$$J_{lm}(E)\sim\frac{Mk^{2l+1}}{4\pi^2\hbar^3}\left\{1-(-1)^l\frac{2(2l+1)(l+|m|)!}{|m|!(l-|m|)!}\times\left(\frac{\beta F}{k}\right)^{3|m|+3}\cos\left[\frac{1}{6}\left(\frac{k}{\beta F}\right)^3+\frac{|m|\pi}{2}\right]\right\}. \tag{52}$$

The modulation is most effective for linear polarization ($m=0$). While being suppressed with respect to the secular part by a factor k^{-3}, its rapidly oscillating behavior still imprints a conspicuous pattern onto the general trend of $J_{l0}(E)$: The current becomes stationary at a series of energy values $E_{\nu l}=[3\pi(4\nu+2l-1)]^{2/3}/8\beta$ (ν integer, $\nu>-l/2$), rendering a "staircase" structure in plots of $J_{l0}(E)$ versus the energy E (see Fig. 3). We note that these stationary values coincide with the appearance of each new dark interference fringe in the center of the corresponding current-density profiles (43) and (45) as predicted by "closed orbit theory" [44].

IV. APPLICATION TO PHOTODETACHMENT PROCESSES

Transcending merely mathematical interest, the multipole wave functions and currents characterizing quantum ballistic motion have been assessed recently in experiment, using electrons accelerated in a homogeneous electric field and ultracold atoms subject to the gravitational force, respectively. In this section, we briefly describe near-threshold photodetachment of negative ions in the presence of an external uniform field. This problem has been studied extensively theoretically (see Refs. [35–38,43–50] and references therein) as well as experimentally [6,7,51–54]. In our opinion, the multipole source model presents the most coherent, and by far the simplest, description of the photodetachment effect. Here, we direct our attention to near-threshold detachment into *p* waves. (The source model for *s*-wave photodetachment in an electric-field environment has been addressed in our previous paper [4].)

A. Photodetachment as a source problem

In the photodetachment setup, a beam of negatively charged ions traverses the focus of a laser beam whose frequency ω closely matches the electron affinity E_0 of the ion. Some ions absorb a laser photon and subsequently emit an electron of energy $E=\hbar\omega-E_0$ into a continuum state to become a neutral atom. In the presence of a homogeneous electric field $\mathbf{F}=-e\mathbf{E}$, these electrons are accelerated towards either a counter, allowing measurement of the total photocurrent $J(E)$ [52–54], or a spatially resolving detector plate that records an image of the photoelectron distribution $j_z(\mathbf{r},\mathbf{o};E)$ [6,7]. (We assume that the ion and laser beams and the electric field are oriented mutually perpendicular, and choose them as the *x*, *y*, and *z* directions of our coordinate system, respectively.)

In the source formalism (Sec. II), the photodetachment phenomenon is interpreted as the scattering of the ionic electrons at the quantized electromagnetic laser field **A**, and the coupling term $W=-e\hbar^2(\mathbf{p}\cdot\mathbf{A})/Mc$ is treated as the interaction potential. Assuming that the external electric field and the laser field do not appreciably disturb the electronic configurations of the initial ionic ground state $|\psi_{\rm ion}\rangle$ and the emerging ground-state neutral atom $|\psi_{\rm atom}\rangle$, we proceed to project these states, leading to an effective inhomogeneous Schrödinger equation for the detached electron (2)

$$\left[E-\frac{\boldsymbol{\pi}^2}{2M}-U_{\rm atom}(\mathbf{r})+Fz\right]\psi(\mathbf{r})=\langle\psi_{\rm atom}|W|\psi_{\rm ion}\rangle, \quad (53)$$

where $\boldsymbol{\pi}=\mathbf{p}+e\mathbf{A}/c$, and $U_{\rm atom}(\mathbf{r})$ denotes the short-range interaction between the emitted electron and the remaining neutral atom which can be neglected in leading approximation. (In the related photoionization effect [38,55], a long-range Coulomb attraction between the emitted electron and the emerging ion prevails which must be included in the external potential: $U_{\rm ext}(\mathbf{r})=Fz-e^2/r$. The additional term renders the treatment of near-threshold photoionization considerably more difficult.) In strong electric fields, the effects of $U_{\rm atom}(\mathbf{r})$ may become important and must be included in a perturbative rescattering series. Similarly, the influence of the oscillating laser field on the electronic motion may be taken into account by a Floquet series expansion. (The electron dynamics in the laser field becomes dominant only for extreme intensities where it causes a wealth of new phenomena, e.g., high-harmonic generation [56,57].) A comprehensive study of these corrections is performed in Ref. [43]. However, for moderate fields and laser intensities, and frequencies close to the detachment threshold, they may be safely ignored.

In order to fit the problem to the ballistic multipole formalism (Sec. III), we approximate the source term $\sigma(\mathbf{r})=\langle\psi_{\rm atom}|W|\psi_{\rm ion}\rangle$ in Eq. (53) by a properly chosen multipole point source (15). To this end, we first note that $\sigma(\mathbf{r})$ is limited in extension to the size of the parent ion and thus is small compared to the initial wavelength of the photoelectron. The details of the source structure then may be condensed into a single parameter, the source strength *C*. (Otherwise, finite-size effects have to be taken into consideration. For Gaussian sources, the deviation from the point source behavior has been studied in detail [4]. See also Sec. V.) This leaves only the multipole character of the source to be determined, which in turn is fixed by the selection rules for dipole radiation. Since emission into channels of higher angular momentum at energies close to threshold is strongly suppressed (as exemplified by the Wigner law (25) for freely propagating particles), only the lowest permissible multipole order is appreciably populated. Usually, this effect leads to isotropic emission of the photoelectron ($l=0$) from the point source [4,6,7,54]. However, if both the parent ion and the emerging neutral atom possess *S* ground states, the photoelectron must carry the spin of the absorbed laser photon and is therefore emitted into a *p* wave, where the distribution onto the various *m* sublevels is determined by the laser polarization vector $\boldsymbol{\epsilon}$:

$$\left[E-\frac{p^2}{2M}+Fz\right]\psi(\mathbf{r})=C(\boldsymbol{\epsilon}\cdot\boldsymbol{\nabla})\,\delta(\mathbf{r})=\sum_{m=-1}^{1}\lambda_{1m}\delta_{1m}(\mathbf{r}). \quad (54)$$

(Most prominently, this occurs in the photodetachment of hydrogen ions H^- first studied experimentally by Bryant *et al.* [51].) The problem then immediately yields to a description in terms of the ballistic multipole waves $G_{10}(\mathbf{r},\mathbf{o};E)$ (39) and $G_{1,\pm1}(\mathbf{r},\mathbf{o};E)$ (40), and results for the ensuing current distributions are presented below.

B. The far-field current profile

Uniform acceleration as a mechanism for two-path interference was first established by Fabrikant [35,45]. Demkov *et al.* [36] improved on his results, and also realized that the fringe pattern in quantum ballistic motion (Sec. III C) should be experimentally observable in near-threshold photodetachment. This assertion was finally confirmed by Blondel *et al.* [6,7] who recorded the photoelectron distribution generated by various ion beams in a homogeneous electric field with a spatially sensitive detector plate and in the course established a new method for the precise determination of electron affinities (''photodetachment microscopy''). For electrical

fields **E** of a few hundred V/m and a source-detector distance $z=0.514$ m, circular fringes with sizes exceeding 1 mm were observed. These experiments were performed on ions that detach electrons into *s*-waves. Due to the low near-threshold photoabsorption rates, photocurrent profiles in *p*-wave detachment so far have not been measured. Yet source theory predicts an interesting dependence (54) of these patterns on the laser polarization $\boldsymbol{\epsilon}$ that is absent in isotropic emission. We discuss some examples below.

First, however, we briefly comment on *s*-wave photodetachment. In this case, the electron is effectively emitted by an isotropic point source $\sigma(\mathbf{r})=C\delta_{00}(\mathbf{r})$, and its wave function is thus proportional to the ballistic Green function $G(\mathbf{r},\mathbf{o};E)$ (27). The distribution of electrons collected on the distant detector hence serves as a measure of the corresponding current density $j^{(z)}(\mathbf{r},\mathbf{o};E)$ (6) which is stated in exact form in Ref. [4], and is in very good agreement with experiment. For large separation of source and detector, a simplified analysis using the far-field approximations (41) and (43) for the ballistic Green function and its current density is equally suited. Assuming a unit strength source ($C=1$), we obtain

$$G_{00}(\mathbf{r},\mathbf{o};E)\sim 4i\beta(\beta F)^3\frac{\mathrm{Ci}(\alpha_+)}{\sqrt{-4\pi\alpha_+}}\mathrm{Ai}(\alpha_-), \tag{55}$$

[where $\alpha_\pm$ is defined in Eq. (28)], while the ensuing current-density matrix element reads

$$j^{(z)}_{00,00}(\mathbf{r},\mathbf{o};E)\sim -\frac{2\beta^6F^5}{\pi^2\hbar\,\alpha_+}\mathrm{Ai}(\alpha_-)^2. \tag{56}$$

For large z, the electron density varies with the radial distance R like the square of the Airy function $\mathrm{Ai}[-2\beta E(1-R^2/R_{\mathrm{cl}}^2)]^2$, where $R_{\mathrm{cl}}^2=4Ez/F$ (see Sec. III C). This formula was used by Blondel *et al.* [7] to analyze their experimental results.

Now we turn to the case of *p*-wave photodetachment. According to Eq. (54), the electron wave function $\psi(\mathbf{r})$ is a superposition of the $l=1$ multipole Green functions $G_{10}(\mathbf{r},\mathbf{o};E)$ (39) and $G_{1,\pm1}(\mathbf{r},\mathbf{o};E)$ (40) whose relative weights depend on the laser polarization $\boldsymbol{\epsilon}$. For our purposes, again their far-field asymptotics (41) suffice,

$$G_{10}(\mathbf{r},\mathbf{o};E)\sim -8\sqrt{3}i\beta(\beta F)^4\frac{\mathrm{Ci}(\alpha_+)}{\sqrt{-4\pi\alpha_+}}\mathrm{Ai}'(\alpha_-), \tag{57}$$

$$G_{1,\pm1}(\mathbf{r},\mathbf{o};E)\sim \pm 4\sqrt{3}\beta(\beta F)^5\frac{\mathrm{Ci}(\alpha_+)}{\sqrt{2\pi\alpha_+}}(x\pm iy)\mathrm{Ai}(\alpha_-). \tag{58}$$

Their associated current-density matrix elements $j^{(z)}_{1m,1m'}(\mathbf{r},\mathbf{o};E)$ are easily evaluated from Eq. (43).

Here, we examine four specific setups of the photodetachment experiment in detail. Since the laser beam points along the y axis, the polarization vector $\boldsymbol{\epsilon}$ is confined to the x-z plane. Some natural choices for it are $\boldsymbol{\epsilon}_\pi=\hat{\boldsymbol{e}}_z$ (parallel or π polarization with respect to the electric field **E**), $\boldsymbol{\epsilon}_\sigma=\hat{\boldsymbol{e}}_x$ (perpendicular or σ orientation), $\boldsymbol{\epsilon}_{\mathrm{circ}}=(\hat{\boldsymbol{e}}_z+i\hat{\boldsymbol{e}}_x)/\sqrt{2}$ (circular polarization), and $\boldsymbol{\epsilon}_{\mathrm{tilt}}=(\hat{\boldsymbol{e}}_z+\hat{\boldsymbol{e}}_x)/\sqrt{2}$ (linearly polarized under an angle of 45° to **E**). The corresponding normalized multipole sources in Eq. (54) read

$$\sigma_\pi(\mathbf{r})=\delta_{10}(\mathbf{r}), \tag{59}$$

$$\sigma_\sigma(\mathbf{r})=-\frac{1}{\sqrt{2}}[\delta_{11}(\mathbf{r})-\delta_{1,-1}(\mathbf{r})], \tag{60}$$

$$\sigma_{\mathrm{circ}}(\mathbf{r})=\frac{1}{2}[-i\delta_{11}(\mathbf{r})+\sqrt{2}\,\delta_{10}(\mathbf{r})+i\delta_{1,-1}(\mathbf{r})], \tag{61}$$

$$\sigma_{\mathrm{tilt}}(\mathbf{r})=\frac{1}{2}[-\delta_{11}(\mathbf{r})+\sqrt{2}\,\delta_{10}(\mathbf{r})+\delta_{1,-1}(\mathbf{r})]. \tag{62}$$

[Note that $\sigma_{\mathrm{circ}}(\mathbf{r})$ and $\sigma_{\mathrm{tilt}}(\mathbf{r})$ only differ in the relative phase of their multipole components.] A brief calculation using Eq. (43) yields the asymptotic photocurrent-density profiles generated by these *p*-wave sources:

$$j^{(z)}_\pi(\mathbf{r},\mathbf{o};E)\sim\frac{24\beta^8F^7}{\pi^2\hbar(-\alpha_+)}\mathrm{Ai}'(\alpha_-)^2, \tag{63}$$

$$j^{(z)}_\sigma(\mathbf{r},\mathbf{o};E)\sim\frac{24\beta^{10}F^9}{\pi^2\hbar\,\alpha_+^2}x^2\mathrm{Ai}(\alpha_-)^2, \tag{64}$$

$$j^{(z)}_{\mathrm{circ}}(\mathbf{r},\mathbf{o};E)\sim\frac{12\beta^8F^7}{\pi^2\hbar(-\alpha_+)}\left(\mathrm{Ai}'(\alpha_-)-\frac{\beta Fx}{\sqrt{-\alpha_+}}\mathrm{Ai}(\alpha_-)\right)^2, \tag{65}$$

$$j^{(z)}_{\mathrm{tilt}}(\mathbf{r},\mathbf{o};E)\sim\frac{12\beta^8F^7}{\pi^2\hbar(-\alpha_+)}\left(\mathrm{Ai}'(\alpha_-)^2+\frac{(\beta Fx)^2}{(-\alpha_+)}\mathrm{Ai}(\alpha_-)^2\right). \tag{66}$$

[In a more involved manner, approximations equivalent to Eqs. (63) and (64) were also derived by Golovinskii [50].]

We now highlight some properties of these distributions. They are depicted in Fig. 2 for the set of parameters used in Blondel's experiment [6], viz., initial electronic energy $E=6.08\times10^{-5}$ eV, electric-field strength $\mathbf{E}=116$ V/m, and detector distance $z=0.514$ m. A concentric arrangement of the interference rings only occurs for π and σ polarization of the laser beam, where the nodes and maxima are interchanged in the respective images, as predicted in Eq. (45). Hence, the fringe pattern encodes information about the orbital structure of the source, in particular, its phase $\gamma(\theta,\phi)$ [36]. (In σ polarization, the underlying interference pattern is the same as in *s*-wave photodetachment [4,7].) Likewise, a sharply defined interference structure is observed for circular polarization $\boldsymbol{\epsilon}_{\mathrm{circ}}$ (65), as this source conforms to the condition outlined in Sec. III C. However, the mirror symmetry $x\rightarrow -x$, present in the other three plots, is conspicuously broken, as the number of fringes differs on the left and right

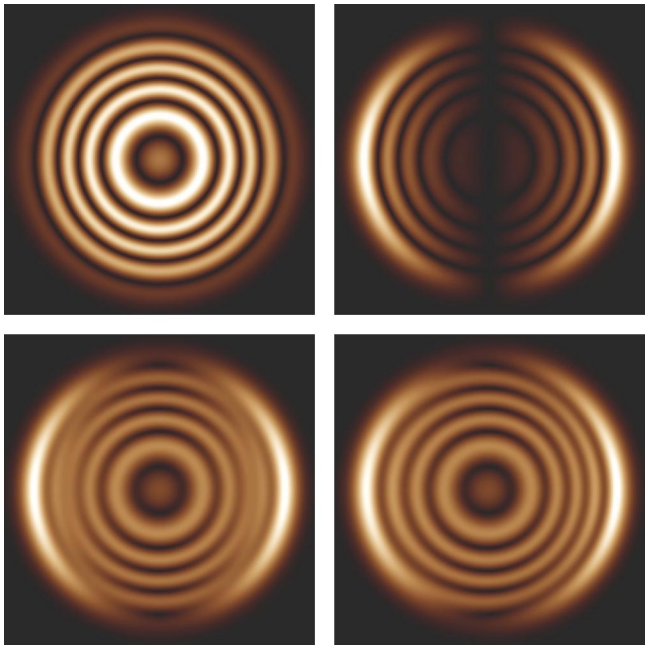

FIG. 2. Photocurrent density profiles in *p*-wave detachment. Clockwise, from left upper image: photoelectron distribution for parallel (63) and perpendicular polarization (64) of the laser beam, profile for circular (65) and linear polarization, tilted under 45° from the direction of field (66). The area displayed in each image is 1.2×1.2 mm^2. Parameters: source-screen distance $z=0.514$ m, initial electronic energy $E=60.8$ μeV, force strength $F=116$ eV/m.

side of the current-density profile. Finally, due to unequal weights $|A(\theta,\phi)|$ of the interfering trajectories, no clear-cut ring pattern is present in the tilted case $\boldsymbol{\epsilon}_{\rm tilt}$. Indeed, Eq. (63)–(66) show that the corresponding image averages the patterns obtained in π and σ polarization: $j^{(z)}_{\rm tilt}(\mathbf{r},\mathbf{o};E)=[j^{(z)}_{\pi}(\mathbf{r},\mathbf{o};E)+j^{(z)}_{\sigma}(\mathbf{r},\mathbf{o};E)]/2$.

C. The total photocurrent

The total detachment rate $J(E)$ of photoelectrons as a function of the electron excess energy E was first examined experimentally by Bryant *et al.* [51], followed by theoretical approaches mostly based either on integral representations of the Green function (27) [46,49] or an analysis using Fermi's golden rule (10) [44,47]. The ballistic multipole source model yields a closed expression for all currents $J_{lm}(E)$ (50), thus obliterating the need for the rather involved calculations in the former approaches.

We again briefly comment on the case of isotropic emission of the photocurrent. For a normalized source ($C=1$), we immediately obtain [4,49,58]

$$J_{00}(E)=\frac{M\beta F}{2\pi\hbar^3}[\mathrm{Ai}'(\epsilon)^2-\epsilon\mathrm{Ai}(\epsilon)^2], \tag{67}$$

where $\epsilon=-2\beta E$ (30). The near-threshold *s*-wave photocurrent spectrum has been recorded with high precision by Gibson *et al.* [52,54] and is in virtually perfect agreement with Eq. (67).

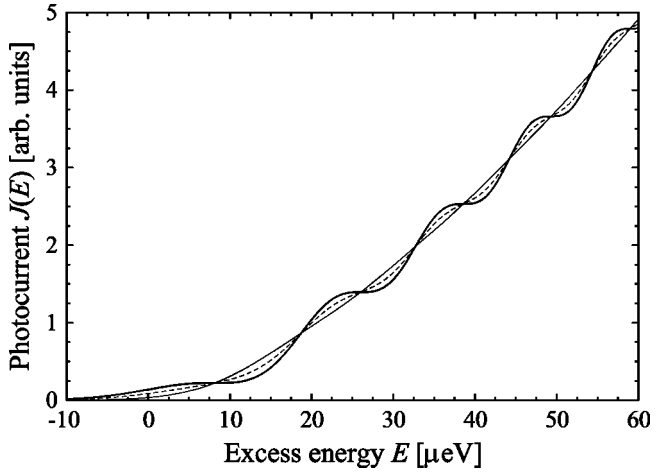

FIG. 3. Total current (in arbitrary units) for *p*-wave photodetachment vs electron excess energy E (in μeV) for an external field $F=116$ eV/m. Bold line, current $J_{10}(E)$ (68), observed in π polarization of the laser beam; light line, $J_{1,\pm1}(E)$ (69), valid for σ polarization. Circular and tilted polarizations (61) and (62) yield the same averaged current (dotted line).

For detachment into a *p* wave, the general formula (50) reduces to the expressions

$$J_{10}(E)=\frac{M(\beta F)^3}{\pi\hbar^3}[2\epsilon^2\mathrm{Ai}(\epsilon)^2-4\mathrm{Ai}(\epsilon)\mathrm{Ai}'(\epsilon)-2\epsilon\mathrm{Ai}'(\epsilon)^2], \tag{68}$$

$$J_{1,\pm1}(E)=\frac{M(\beta F)^3}{\pi\hbar^3}[2\epsilon^2\mathrm{Ai}(\epsilon)^2-\mathrm{Ai}(\epsilon)\mathrm{Ai}'(\epsilon)-2\epsilon\mathrm{Ai}'(\epsilon)^2], \tag{69}$$

which differ merely in a single prefactor. These currents were first obtained via Fermi's golden rule (10) by Slonim and Dalidchik [43,59], while integral representations are listed in Refs. [44,47,53]. Within the error margins, both expressions again reproduce the experimental *p*-wave detachment spectrum by Gibson *et al.* [53].

Due to the cylindrical symmetry of the potential, the total photocurrent $J(E)$ reduces to a linear combination of Eqs. (68) and (69) for arbitrary orientation of the polarization vector $\boldsymbol{\epsilon}$ (see Sec. II B). In particular, the current $J_{10}(E)$ is observed in π polarization ($\boldsymbol{\epsilon}\|\mathbf{E}$), while $J_{1,\pm1}(E)$ prevails in σ polarization ($\boldsymbol{\epsilon}\perp\mathbf{E}$). In both the tilted and circular polarizations of the laser beam stated in Eqs. (61) and (62), the multipole currents contribute equal weight: $J_{\rm circ}(E)=J_{\rm tilt}(E)=[J_{10}(E)+J_{1,\pm1}(E)]/2$. For illustration, these currents are plotted in Fig. 3. While generally following their low-field limit given by the *p*-wave Wigner law $J(E)\propto E^{3/2}$ (25), a strong ''staircase'' modulation is observed in π polarization that is absent for the σ case, as predicted in Sec. III D.

V. ATOM LASER WITH ROTATING SOURCE

In an earlier paper [4], we devised a source model for an atom laser supplied by an ideal BEC. Let us first summarize some of the results obtained there before we set out to extend the theory to higher multipoles: We consider a two-state model for the atom laser, where one magnetically trapped state (the BEC, acting as a quantum source) is weakly coupled to a nontrapped state (the atom laser) by a monochromatic radio-frequency field. (Replenishing the source condensate to maintain a truly stationary flux in the atom laser poses difficult technical problems [60].) We are interested in the propagation of atoms coherently released from the condensate in the surrounding gravitational field. For a N-particle BEC of isotropic Gaussian shape,

$$\sigma(\mathbf{r}) = \sqrt{N}\hbar\Omega a^{-3/2}\pi^{-3/4}e^{-r^2/2a^2} \tag{70}$$

(where $\hbar\Omega$ denotes the interaction strength), we found an explicit expression for the resulting beam wave function $\psi(\mathbf{r}) = \int d^3\mathbf{r}'\, G(\mathbf{r},\mathbf{r}';E)\sigma(\mathbf{r}')$ [4] that is closely related to the ballistic Green function (27) itself. Remarkably, in the far-field sector a ballistic Gaussian source may be replaced by a virtual point source at a position displaced from its center in the direction of force $\mathbf{F}$. With respect to this virtual source, we introduce a set of shifted variables depending on the scaled condensate width $\alpha = \beta F a$ [where β is defined in Eq. (29)], and $\mathbf{F} = mg\hat{\mathbf{e}}_z$ now represents the gravitational force on a BEC atom

$$\tilde{\zeta} = \zeta + 2\alpha^4, \quad \tilde{\rho}^2 = \xi^2 + \upsilon^2 + \tilde{\zeta}^2, \quad \tilde{\epsilon} = \epsilon + 4\alpha^4. \tag{71}$$

Using these variables, the wave function of the atomic beam $\psi(\mathbf{r})$ (4) and the total current $J_{\rm tot}(E)$ (7) carried by it are conveniently expressed in terms of the special functions $Q_k(\tilde{\rho},\tilde{\zeta};\tilde{\epsilon})$ (37) and $\mathrm{Qi}_k(\tilde{\epsilon})$ (49) discussed in Appendix B (cf. Ref. [4]):

$$\psi(\mathbf{r}) = -4\beta(\beta F)^3\Lambda(\tilde{\epsilon})Q_1(\tilde{\rho},\tilde{\zeta};\tilde{\epsilon}), \tag{72}$$

$$J_{\rm tot}(E) = \frac{8}{\hbar}\beta(\beta F)^3\Lambda(\tilde{\epsilon})^2\mathrm{Qi}_1(\tilde{\epsilon}). \tag{73}$$

We note that the virtual source strength $\Lambda(\tilde{\epsilon})$ is strongly energy and size dependent,

$$\Lambda(\tilde{\epsilon}) = \sqrt{N}\hbar\Omega(2\sqrt{\pi}a)^{3/2}e^{2\alpha^2(\tilde{\epsilon}-4\alpha^4/3)}. \tag{74}$$

Below, we use the multipole formalism to obtain closed solutions for Gaussian sources with angular momentum. These states naturally arise in a rotating condensate. For simplicity, we assume that the rotating BEC quantum fluid is in its thermodynamical ground state, where it exhibits a set of vortices (at least, one) symmetrically arranged in an extended lattice structure [11].

A. Ideal atom laser from a single vortex

Here, we examine the atom laser beam arising in the presence of a single vortex with fixed direction in a noninteracting boson gas in an isotropic trap. The wave function of the rotating condensate is then given by a first excited radial harmonic-oscillator state [61] and drops to zero along the vortex line. (In practice, the vortex line is not stationary, but may precess slowly in time [62].) For simplicity, we will first align the vortex to the direction of force $\hat{\boldsymbol{e}}_z$. The source wave function $\sigma_{11}(\mathbf{r})$ is then the oscillator eigenstate with angular momentum $l=m=1$. In analogy to the multipole source formalism (Sec. II B), application of the corresponding spherical tensor gradient $K_{11}(\boldsymbol{\nabla})$ (13) to the vortex-free BEC ground state (70) yields this source function

$$\sigma_{11}(\mathbf{r}) = N_1 K_{11}(\boldsymbol{\nabla})\sigma(\mathbf{r}) = \frac{\sqrt{N}\hbar\Omega}{a^{5/2}\pi^{3/4}}(x+iy)e^{-r^2/2a^2}, \tag{75}$$

with $N_1 = a\sqrt{8\pi/3}$. In general, we define Gaussian multipole sources $\sigma_{lm}(\mathbf{r})$ analogous to Eq. (15) via

$$\sigma_{lm}(\mathbf{r}) = N_l K_{lm}(\boldsymbol{\nabla})\sigma(\mathbf{r}), \tag{76}$$

where $N_l^2 = 2\pi^{3/2}a^{2l}/\Gamma(l+3/2)$ is obtained from the normalization condition $\int d^3r|\sigma_{lm}(\mathbf{r})|^2 = N(\hbar\Omega)^2$. The source functions thus generated turn out to be the lowest-lying oscillator eigenstates of (l,m) spherical symmetry [with energy $E = (l+3/2)\hbar^2/Ma^2$]. [In particular, $\sigma_{00}(\mathbf{r}) = \sigma(\mathbf{r})$ covers the isotropic Gaussian source (70).] From Eq. (4), we evaluate the wave function $\psi_{lm}(\mathbf{r})$ of the corresponding outcoupled state:

$$\psi_{lm}(\mathbf{r}) = (-1)^l N_l \int d^3r'\,\sigma(\mathbf{r}')K_{lm}(\boldsymbol{\nabla}')G(\mathbf{r},\mathbf{r}';E). \tag{77}$$

Here, we integrated by parts to shift the spherical tensor operator to the Green function (27). The substitution rule (34) then enables us to further evaluate the integral in terms of derivatives of the known atom laser wave function for zero angular momentum $\psi(\mathbf{r})$ (72):

$$\psi_{lm}(\mathbf{r}) = N_l K_{lm}[\partial_x, \partial_y, \partial_z - F\partial_E]\psi(\mathbf{r}). \tag{78}$$

Via the differentiation rules (B3) and (B4), we may reduce these derivatives to a sum of the auxiliary functions $Q_k(\tilde{\rho},\tilde{\zeta};\tilde{\epsilon})$ (B1), analogous to the case of multipole point sources $\delta_{lm}(\mathbf{r})$ (38). For a single vortex, it suffices to consider the sources $\sigma_{1m}(\mathbf{r})$ with $l=1$, $|m|=0,1$,

$$\psi_{10}(\boldsymbol{\rho}) = 4\sqrt{2}\beta(\beta F)^3\alpha\Lambda(\tilde{\epsilon})[2\tilde{\zeta}Q_2(\tilde{\rho},\tilde{\zeta};\tilde{\epsilon}) - 4\alpha^2 Q_1(\tilde{\rho},\tilde{\zeta};\tilde{\epsilon}) + Q_0(\tilde{\rho},\tilde{\zeta};\tilde{\epsilon})], \tag{79}$$

$$\psi_{1\pm1}(\boldsymbol{\rho}) = \mp 8\beta(\beta F)^3\alpha\Lambda(\tilde{\epsilon})(\tilde{\xi}\pm i\tilde{\upsilon})Q_2(\tilde{\rho},\tilde{\zeta};\tilde{\epsilon}). \tag{80}$$

[For $\alpha\to 0$, point sources are recovered, and Eqs. (79) and (80) become proportional to the p-wave multipole Green functions (39) and (40).] Note that $\psi_{1\pm1}(\boldsymbol{\rho})$ vanishes on the z axis: For parallel orientation of vortex and force, the vortex line is preserved in the atom laser profile.

In analogy to Sec. III D, we calculate the overall outcoupling rate as a function of the radiation frequency detuning ($E=h\Delta\nu$). According to Eq. (8), the total multipole current is available from $J_{lm}(E)=-2\,\mathrm{Im}[\langle\sigma_{lm}|G|\sigma_{lm}\rangle]/\hbar$. In practice, the calculation is best carried out in momentum space, where both the Gaussian multipole source (76) and the ballistic propagator (32) take on a particularly simple form. Like the point-source currents (50) (to which they reduce as $\alpha\to 0$), the Gaussian multipole currents are expressed using the auxiliary functions $\mathrm{Qi}_k(\tilde{\epsilon})$ (49) covered in Appendix B 2. Within the $l=1$ triplet, they explicitly read

$$J_{10}(\tilde{\epsilon})=\frac{32}{\hbar}\beta(\beta F)^3\alpha^2\Lambda(\tilde{\epsilon})^2[\mathrm{Qi}_2(\tilde{\epsilon})+8\alpha^4\mathrm{Qi}_1(\tilde{\epsilon}) -4\alpha^2\mathrm{Qi}_0(\tilde{\epsilon})+\tfrac{1}{2}\mathrm{Qi}_{-1}(\tilde{\epsilon})], \tag{81}$$

$$J_{1\pm1}(\tilde{\epsilon})=\frac{32}{\hbar}\beta(\beta F)^3\alpha^2\Lambda(\tilde{\epsilon})^2\mathrm{Qi}_2(\tilde{\epsilon}). \tag{82}$$

Thanks to the preserved rotational symmetry of the system, all total current matrix elements $J_{lm,l'm'}(\tilde{\epsilon})$ with $m\neq m'$ vanish, as indicated in Sec. II B.

For extended condensates ($\alpha\gg 1$), we may replace the functions $\mathrm{Qi}_k(\tilde{\epsilon})$ by their asymptotic series (B12). Further expanding the currents around their maximum near $\epsilon=0$, we obtain their large-source approximations

$$J_{10}(\tilde{\epsilon})\sim N\sqrt{\pi}\beta\hbar\Omega^2\frac{\epsilon^2}{\alpha^3}e^{-\epsilon^2/4\alpha^2}, \tag{83}$$

$$J_{1\pm1}(\tilde{\epsilon})\sim 2N\sqrt{\pi}\hbar\Omega^2\frac{\beta}{\alpha}e^{-\epsilon^2/4\alpha^2}. \tag{84}$$

As expected from our earlier results for a simple Gaussian source [4], these currents can be interpreted as the integrated condensate density along a slice through the BEC at a height z fixed by the ''resonance condition'' $E+Fz=0$ (Franck-Condon principle):

$$J_{lm}(E)\sim\frac{2\pi}{\hbar}\int d^3\mathbf{r}|\sigma_{lm}(\mathbf{r})|^2\delta(E+Fz). \tag{85}$$

(A semiclassical derivation of the ''slicing approximation'' is presented in Ref. [63].) Equation (85) evidently fulfils the sum rule (9) for the total outcoupling rate.

For illustration, we consider two orientations of the vortex with respect to the gravitational force **F**. A vortex parallel to the field is simply represented by the Gaussian condensate wave function $\sigma_{11}(\mathbf{r})$ Eqs. (75), and the ensuing laser beam characteristics are expressed in Eqs. (80) and (82). We also examine the case of a vortex along the x axis, i.e., perpendicular to **F**. The corresponding BEC source function $\sigma_{1\perp}(\mathbf{r})$ is connected to the parallel vortex model by a rotation $\exp(-i\pi\hat{L}_y/2)$. Application of the $l=1$ rotation matrix for angular-momentum eigenstates [64] yields the following source term [cf. Eq. (61)]:

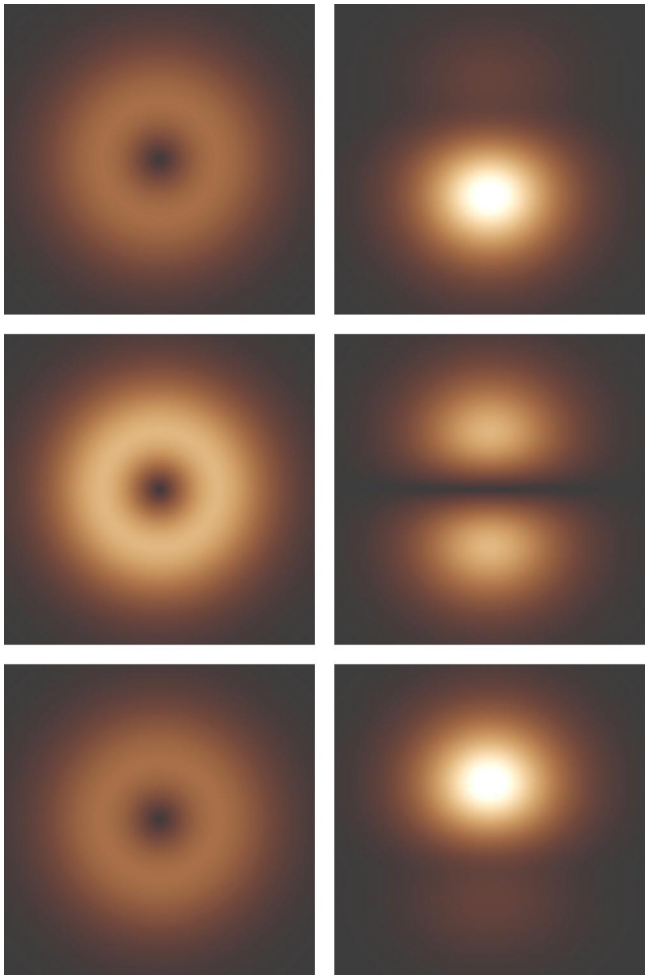

FIG. 4. Atom laser density profiles for a rotating ^{87}Rb BEC source sustaining one vortex. Left column: parallel orientation of vortex line and force **F**, with source $\sigma_{11}(\mathbf{r})$ (75). Right column: vortex perpendicular to **F**, as given by $\sigma_{1\perp}(\mathbf{r})$ (86). The detuning frequencies $\Delta\nu$ are -4 kHz (top row), 0 kHz (center row), and $+4$ kHz (bottom row), respectively. The brightest spots of the distribution pertain to a density of 2.5 atoms/μm^3. Displayed area, 30×30 μm^2; distance from source, $z=1$ mm: source parameters, $a=2$ μm, $\Omega=2\pi\times 100$ Hz, $N=10^6$ atoms.

$$\sigma_{1\perp}(\mathbf{r})=\frac{1}{2}[\sigma_{11}(\mathbf{r})+\sqrt{2}\sigma_{10}(\mathbf{r})+\sigma_{1,-1}(\mathbf{r})], \tag{86}$$

with a corresponding superposition of Eqs. (79), and (80) as beam wave function $\psi_{1\perp}(\mathbf{r})$ and an associated total current,

$$J_{1\perp}(\tilde{\epsilon})=\frac{1}{2}[J_{10}(\tilde{\epsilon})+J_{1,\pm1}(\tilde{\epsilon})]. \tag{87}$$

Figure 4 depicts atom laser density profiles generated by an ideal ^{87}Rb BEC of width $a=2$ μm at a distance $z=1$ mm in the center of the resonance ($\Delta\nu=0$ kHz) as well as for positive and negative detuning ($\Delta\nu=\pm 4$ kHz). For this choice of parameters, $\alpha\approx 3.33$, so the effective energy $\tilde{\epsilon}=4\alpha^4$ (71) of the assigned virtual point source indicates tunneling emission. According to the results presented in Sec. III C, we

expect density profiles of overall Gaussian shape, with a mean width $D(z)=2\tilde{z}/\tilde{\kappa}$ (47), where $\tilde{z}=(\zeta+2\alpha^4)/\beta F$ and $\tilde{\kappa}=4\beta F\alpha^2$ denote the distance from the virtual source and the virtual evanescent wave number, respectively. (Alternatively, this result follows from the spreading of a minimal uncertainty wave packet of initial width a during its time of flight $T=\sqrt{2Mz/F}$ [5].) This Gaussian envelope is modulated by a factor $f(\xi,\upsilon)$ that depends on the relative orientation of the vortex and the gravitational force. A fairly cumbersome calculation yields for the asymptotic shape of the density profiles generated by the sources (75) and (86) in the far-field sector, valid for $\alpha\gg 1$,

$$\rho(\xi,\upsilon)\sim 16N(\hbar\Omega)^2\beta^5F^3\alpha^3\frac{f(\xi,\upsilon)}{\sqrt{2\pi\zeta}(\zeta+2\alpha^4)^2}\times\exp\left[-\left(\frac{\epsilon^2}{4\alpha^2}+\frac{2\alpha^2(\xi^2+\upsilon^2)}{\zeta+2\alpha^4}\right)\right], \tag{88}$$

where the modulation factors $f_{11}(\xi,\upsilon)$ and $f_{1\perp}(\xi,\upsilon)$ for parallel and perpendicular orientation read, respectively,

$$f_{11}(\xi,\upsilon)=\xi^2+\upsilon^2,\quad f_{1\perp}(\xi,\upsilon)=\frac{\epsilon^2}{4}+\left(\upsilon-\frac{\epsilon\sqrt{\zeta}}{2\sqrt{2}\alpha^2}\right)^2. \tag{89}$$

[We used the dimensionless coordinates introduced in Eq. (30).] Clearly, $f_{11}(\xi,\upsilon)$ effects the propagation of the vortex in the parallel case. However, the dependence of $f_{1\perp}(\xi,\upsilon)$ on the source distance ζ and the detuning $\Delta\nu=-\epsilon/2h\beta$ renders the atom laser profiles generated in perpendicular orientation more intriguing (see Fig. 4): The detuning-dependent, isotropic contribution $\epsilon^2/4$ competes with a shifted parabolic term that grows linearly with the detector distance ζ. For $\zeta\ll 2\alpha^4$, detuning blurs the simple vortex image present at center resonance, while for $\zeta\gg 2\alpha^4$ the latter term in Eq. (89) dominates, causing the appearance of a node line in the profile whose relative position shifts linearly with the detuning ν. The transition between these markedly different regimes of the atom laser occurs at considerable distance from the BEC. In our example, $\zeta=2\alpha^4$ holds at a separation $z_{\rm tr}\approx 150\ \mu$m, so the far-field behavior is shown in Fig. 4. However, for larger sources, this characteristic distance quickly reaches macroscopic dimensions: For $a=10\ \mu$m, we find $z_{\rm tr}\approx 10$ cm.

We now turn to the frequency dependence of the total outcoupling rate. Since $\alpha\gg 1$, use of the asymptotic description (85) is in order. In Fig. 5, we show the resulting current characteristics for both condensate orientations. While in parallel orientation the current distribution is simply Gaussian, it features a dip in the total current at $\Delta\nu=0$ for a vortex line perpendicular to the gravitational field. This behavior is easily understood from Eq. (85): Due to the presence of the vortex line in the slicing plane, at $z=0$ the condensate density adopts a minimum. We note that the slicing approximation fails for small condensates (with $\alpha\sim 1$) and it becomes necessary to use the exact results (81) and (82). The transition between both regimes is studied in detail in Ref. [4].

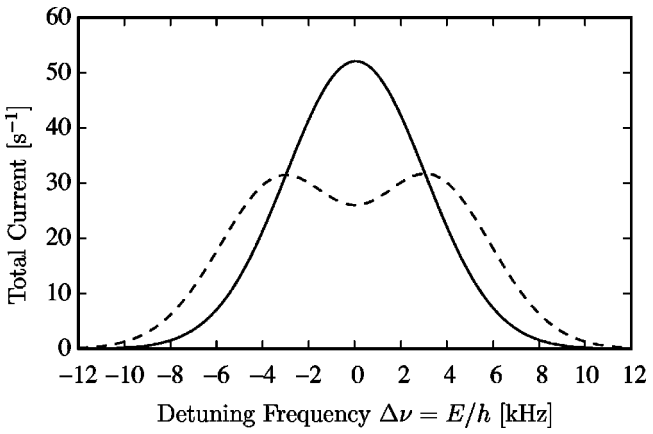

FIG. 5. Total current generated per atom in a ^{87}Rb BEC with one vortex as a function of the detuning frequency $\Delta\nu$. Solid line: vortex line parallel to the gravitational field **F**. Dashed line: vortex line perpendicular to **F**. Parameters: $a=2\ \mu$m, $\Omega=2\pi\times 100$ Hz.

B. Vortex lattices

Using the tools developed in the preceding section, we proceed to give an example of a multipole source where larger values of the angular momentum are present. Rotating Bose-Einstein condensates show superfluid behavior and respond to an externally induced rotation by formation of a vortex lattice [10–12,65]. (For a review on vortices in BECs, see Ref. [61].) No attempt at a description of the formation and parameters of this lattice will be made. Rather, we present a theoretical model for a stationary atom laser supplied by an already formed vortex lattice, with vortex lines oriented parallel to the gravitational field **F**. The wave function of the lattice state (the laser source) is most conveniently modeled in the rotating reference frame (RF), where it becomes time independent; we denote it by $\sigma_{\rm latt,rf}(\mathbf{r})$. However, the laser is observed in the laboratory frame (LF) and hence we first discuss the transformation between both frames.

In the lab frame, the RF source function $\sigma_{\rm latt,rf}(\mathbf{r})$ becomes explicitly time dependent. The transformation between both frames of reference involves a uniform rotation around the z axis with frequency $\Omega_{\rm rot}$, which is generated by the unitary operator $\exp(-iL_z\Omega_{\rm rot}t/\hbar)$. The full time-dependent LF source term consequently reads $\sigma_{\rm latt,lf}(\mathbf{r},t)=e^{-iEt/\hbar}e^{-iL_z\Omega_{\rm rot}t/\hbar}\sigma_{\rm latt,rf}(\mathbf{r})$. Here, decomposition of the source $\sigma_{\rm latt,rf}(\mathbf{r})$ into a superposition of eigenstates $\sigma_{m,\rm rf}(\mathbf{r})$ of L_z makes sense:

$$\sigma_{\rm latt,rf}(\mathbf{r})=\sum_m\ \sigma_{m,\rm rf}(\mathbf{r}). \tag{90}$$

Thus, in the laboratory frame, the rotating source function appears split into stationary components $\sigma_{m,\rm rf}(\mathbf{r})$ shifted in energy. With $E_m=E+m\hbar\Omega_{\rm rot}$, we obtain

$$\sigma_{\rm latt,lf}(\mathbf{r},t)=\sum_m\ e^{-iE_mt/\hbar}\sigma_{m,\rm rf}(\mathbf{r}). \tag{91}$$

The laser wave function resulting from a time-dependent source in the presence of the gravitational field is generated by the ballistic propagator (31):

$$\psi_{\mathrm{latt,lf}}(\mathbf{r},t)=-\frac{i}{\hbar}\int d^3\mathbf{r}'\int_{-\infty}^{t}dt'K(\mathbf{r},t|\mathbf{r}',t')\sigma_{\mathrm{latt,lf}}(\mathbf{r}',t'). \tag{92}$$

The propagator representation of the ballistic Green function (31) then finally yields the beam wave function

$$\psi_{\mathrm{latt,lf}}(\mathbf{r},t)=\sum_m e^{-iE_mt/\hbar}\psi_{m,\mathrm{rf}}(\mathbf{r}), \tag{93}$$

where $\psi_{m,\mathrm{rf}}(\mathbf{r})=\int d^3\mathbf{r}'G(\mathbf{r},\mathbf{r}';E_m)\sigma_{m,\mathrm{rf}}(\mathbf{r}')$ (4). The rotating source function thus allows a description in terms of $G(\mathbf{r},\mathbf{r}';E)$ (Sec. III). We note that both $\psi_{m,\mathrm{rf}}(\mathbf{r})$ and its source $\sigma_{m,\mathrm{lf}}(\mathbf{r})$ are eigenfunctions of L_z: Like the BEC, the atomic beam profile rotates uniformly with frequency Ω_{rot}.

Next, we characterize the source function $\sigma_{\mathrm{latt,rf}}(\mathbf{r})$ for the vortex lattice. This state of the BEC is commonly described as a superposition of angular-momentum eigenstates of the harmonic oscillator [66,67]. The number of vortices and their positions are available from minimizing the energy functional in the rotating frame. For a parallel arrangement of vortices and field **F**, we may model the vortex state as a product of a two-dimensional "lattice function" $\sigma_{2D}(x,y)$ detailing the vortex positions (x_k,y_k) with a Gaussian envelope enforced by the harmonic trap potential. Introducing complex coefficients $v_k=x_k+iy_k$, the lattice function is obtained as a product involving all vortex positions that alternatively may be expressed as a polynomial in $(x+iy)$,

$$\sigma_{2D}(x,y)=\prod_{k=1}^{n}[(x+iy)-v_k]=\sum_{k=0}^{n}w_k^{(n)}(x+iy)^k. \tag{94}$$

The coefficients v_k and w_k are linked via the recursion relation $w_k^{(n)}=w_{k-1}^{(n-1)}-v_{k+1}w_k^{(n-1)}$ $(w_0^{(0)}=1)$. (Usually, these lattices possess elements of symmetry which enforce selection rules on the w_k, leaving only few nonvanishing coefficients.) The complete three-dimensional source function in the rotating frame then reads

$$\sigma_{\mathrm{latt,rf}}(\mathbf{r})=N_n\exp\left(-\frac{x^2+y^2}{2a_x^2}-\frac{z^2}{2a_z^2}\right)\sigma_{2D}(x,y). \tag{95}$$

The constant N_n is determined by the normalization condition $\int d^3\mathbf{r}|\sigma(\mathbf{r})_{\mathrm{latt,rf}}|^2=N(\hbar\Omega)^2$:

$$N_n=\frac{\sqrt{N}\hbar\Omega}{\pi^{3/4}\sqrt{a_z\sum_{k=0}^{n}k!|w_k^{(n)}|^2a_x^{2k+2}}}. \tag{96}$$

Equation (94) then yields the decomposition of $\sigma_{\mathrm{latt,rf}}(\mathbf{r})$ into eigenstates $\sigma_{m,\mathrm{rf}}(\mathbf{r})$ of L_z (90):

$$\sigma_{m,\mathrm{rf}}(\mathbf{r})=N_nw_m^{(n)}(x+iy)^m\exp\left(-\frac{x^2+y^2}{2a_x^2}-\frac{z^2}{2a_z^2}\right). \tag{97}$$

Thus, all $n+1$ source components are eigenstates of the harmonic trap potential, and the highest quantum number m equals the number of vortices present in the BEC.

For the special case of an isotropic trap $(a_x=a_z=a)$, the theory outlined in the preceding section provides both outcoupling rate and beam profile in analytic form. Since the components $\sigma_{m,\mathrm{rf}}(\mathbf{r})$ (97) then simultaneously present eigenstates of L_z and the total angular momentum L^2 with quantum number $l=m$, the source is entirely made up of circular Gaussian multipole states $\sigma_{mm}(\mathbf{r})=N_mK_{mm}(\boldsymbol{\nabla})\sigma(\mathbf{r})$ (70) and (76):

$$\sigma_{m,\mathrm{rf}}(\mathbf{r})=C_n\sqrt{m!}w_m^{(n)}a^m\sigma_{mm}(\mathbf{r}). \tag{98}$$

(Here, we set $C_n^2=[\Sigma_{k=0}^{n}k!|w_k^{(n)}|^2a^{2k}]^{-1}$.) According to Eq. (93), the rotating beam is thus produced by a weighed superposition of stationary sources $\sigma_{mm}(\mathbf{r})$ with effective energy $E_m=E+m\hbar\Omega_{\mathrm{rot}}$. As explained in the introduction to Sec. V, outside the source region each Gaussian multipole source $\sigma_{lm}(\mathbf{r})$ (76) may be mapped onto a corresponding displaced virtual point source of adjusted strength $\Lambda(\tilde{\epsilon})$. This allows to calculate the wave function $\psi_{mm}(\mathbf{r})$ generated by $\sigma_{mm}(\mathbf{r})$ along the lines presented in Sec. III B, and the final result closely resembles the corresponding ballistic multipole Green function $G_{mm}(\mathbf{r},\mathbf{0};E)$ (38):

$$\psi_{mm}(\mathbf{r})=-\frac{4\beta(\beta F)^3}{\sqrt{m!}}\Lambda(\tilde{\epsilon}_m)[2\alpha(\xi+i\upsilon)]^mQ_{m+1}(\tilde{\rho},\tilde{\zeta};\tilde{\epsilon}_m), \tag{99}$$

where $\tilde{\epsilon}_m=-2\beta E_m+4\alpha^4$ (71). Similarly, the total current $J_{mm}(E_m)$ generated by $\sigma_{mm}(\mathbf{r})$ is available from a calculation in the spirit of Sec. III D:

$$J_{mm}(E_m)=\frac{8}{\hbar}\beta(\beta F)^3(2\alpha)^{2m}\Lambda(\tilde{\epsilon}_m)^2\mathrm{Qi}_{m+1}(\tilde{\epsilon}_m). \tag{100}$$

[For $m=0,1$, these expressions reduce to the results (72) and (73) and (80) and (82) presented above.] Substituting Eqs. (98) and (99) in Eq. (93), the wave function of the rotating atom laser beam ultimately reads

$$\psi_{\mathrm{latt,lf}}(\mathbf{r},t)=C_n\sum_{m=0}^{n}e^{-iE_mt/\hbar}\sqrt{m!}w_m^{(n)}a^m\psi_{mm}(\mathbf{r}). \tag{101}$$

Due to cylindrical symmetry, all elements of the total current matrix $J_{lm,l'm'}(E)$ (24) with $m\neq m'$ vanish (see Sec. II B). Therefore, the (stationary) outcoupling rate $J_{\mathrm{latt}}(E)$ reduces to a properly weighed sum of the ballistic multipole currents $J_{mm}(E_m)$ (100):

$$J_{\mathrm{latt}}(E)=C_n^2\sum_{m=0}^{n}m!|w_m^{(n)}|^2a^{2m}J_{mm}(E_m). \tag{102}$$

We illustrate these results using a model condensate featuring a symmetrical triangular lattice of 37 vortices 10 μm apart, embedded into a Gaussian source of width a

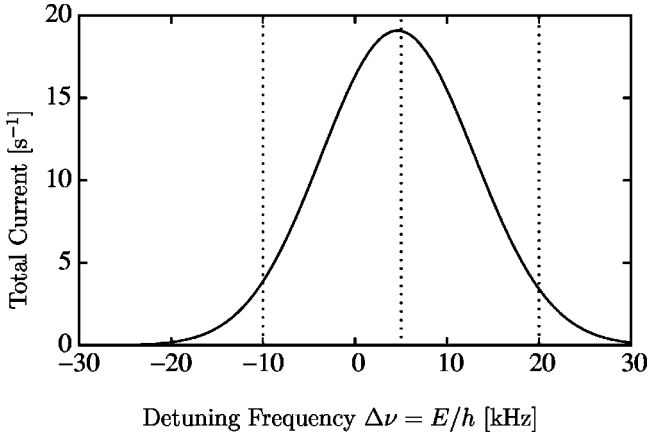

FIG. 6. Total current per atom in a ^{87}Rb BEC with 37 vortices as a function of detuning frequency $\Delta\nu$. The vortex structure of the BEC is not visible in the integrated current. Vortex separation in the BEC: 10 μm, rotation frequency $\Omega_{\rm rot}=2\pi\times250$ Hz, outcoupling strength $\Omega=2\pi\times100$ Hz, size parameter $a=5$ μm.

$=5$ μm. While the frequency dependence of the outcoupling rate merely shows the familiar Gaussian character (compare Figs. 5 and 6), plots of the resulting atom laser profile exhibit rich detail (Fig. 7): Tracing the rotation of the source, the vortex pattern, which is fully transferred from the BEC into the laser beam, forms an intertwined braidlike structure along the z axis. It modulates the lateral beam profile which now strongly depends on the detuning frequency $\Delta\nu$. The outcoupling rate varies between the different angular-momentum components $\sigma_{m,\rm rf}(\mathbf{r})$ (98) that make up the source, as explained in Sec. III C (47). A negative shift in the frequency suppresses states with high $|m|$, leading to an approximate Gaussian shape of the laser profile, whereas positive detuning ($\Delta\nu>0$) emphasizes these contributions. The centrifugal barrier effective for them then produces a ringlike ''crown'' emission pattern.

VI. CONCLUSION

In our study, we established a systematic approach to scattering processes that involve nonisotropic emission of quantum particles. Starting from the stationary Schrödinger equation (2) that incorporates a source term $\sigma(\mathbf{r})$ responsible for a steady particle flow, we proceeded by analogy with potential theory and introduced pointlike ''multipole sources'' $\delta_{lm}(\mathbf{r})$ as limiting cases of sources with (l,m) orbital symmetry. These sources, and the scattering waves and currents generated by them, are available from the conventional Dirac δ singularity and its assigned Green function $G(\mathbf{r},\mathbf{r}';E)$ (3) by application of a differentiation operator of suitable spherical symmetry, the spherical tensor gradient $K_{lm}(\boldsymbol{\nabla}')$ (Sec. II B). The scattering waves emitted by multipole sources locally show pure (l,m) angular symmetry, and in the absence of an external potential, they reduce to the spherical partial waves familiar from conventional scattering theory.

These local-orbital characteristics remain preserved in an external potential that breaks rotational symmetry. The multipole waves then describe the propagation of particles initially emitted in the (l,m) eigenstate of angular momentum, and thus generalize the notion of a partial wave. We performed a detailed study of the linear potential environment $U(\mathbf{r})=-\mathbf{r}\cdot\mathbf{F}$, i.e., scattering in the presence of a uniform force field $\mathbf{F}$. This problem allows for an analytical solution, and closed-form expressions for the ballistic multipole waves $G_{lm}(\mathbf{r},\mathbf{o};E)$ (38) and currents $J_{lm,l'm'}(E)$ (50) are assembled in Sec. III. Uniformly accelerated scattering waves display a characteristic set of features, including a prominent fringe structure and a modulation of the cross section, that semiclassically are attributed to two-path interference in the force field, as well as ballistic tunneling.

The theory of ballistic multipole waves directly applies to near-threshold photodetachment processes in an electric-field environment, a topic that recently attracted considerable interest. The source model directly yields analytical expres-

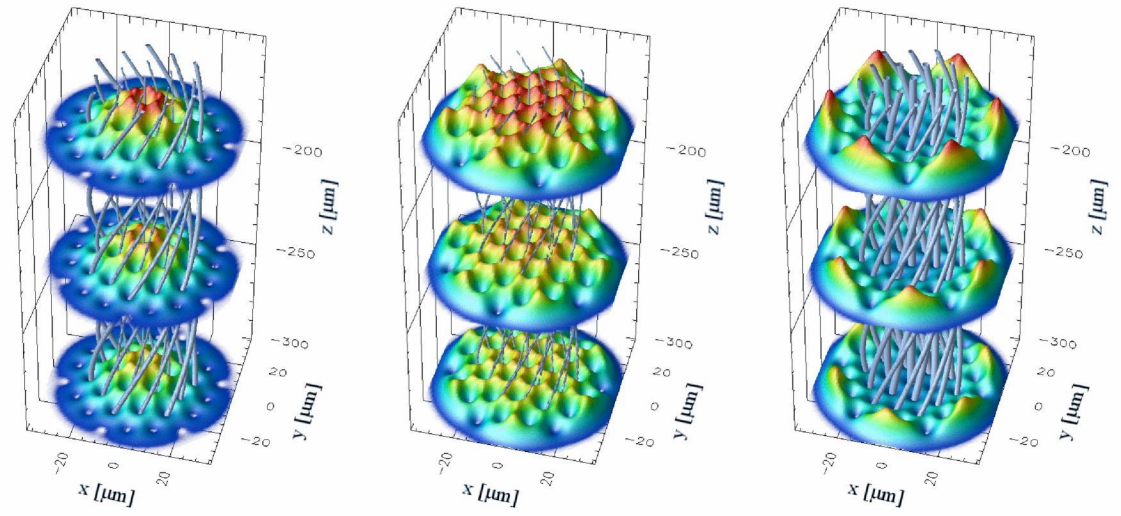

FIG. 7. Beam profiles of an atom laser generated by a rotating BEC sustaining a triangular 37-vortex lattice. From left to right, we vary the detuning frequency: $\Delta\nu=-10$ kHz, 5 kHz, 20 kHz, as marked by dotted lines in Fig. 6. The density in the beam is plotted at three different distances $z=177$ μm, 239 μm, 300 μm from the center of the BEC. The vortex cores are indicated by small tubes at all distances. BEC parameters same as Fig. 6.

sions for the photocurrent spectrum and the spatial electron distribution that are in excellent agreement with the available experimental data. Our attention was mainly dedicated to *p*-wave photodetachment, where we discussed the influence of the laser polarization on the photoelectron current profile (Sec. IV).

Somewhat akin to the situation in potential theory, in the ballistic environment extended sources of Gaussian shape may be replaced by ''virtual'' point sources that are shifted from the center of the actual distribution. This mapping remains feasible for ''Gaussian multipole sources'' $\sigma_{lm}(\mathbf{r})$ (76), harmonic-oscillator eigenstates of (l,m) orbital symmetry that are generated by the same differentiation formalism as the multipole point sources $\delta_{lm}(\mathbf{r})$. Depending on their size, these Gaussian multipoles may act as effective ballistic tunneling sources that display unusual properties. In practice, Gaussian wave functions are shared by the atoms in an ideal Bose-Einstein condensate trapped in a harmonic potential. A ballistic tunneling source is then realized by continuous outcoupling of atoms under the influence of gravity, leading to the formation of an ''atom laser'' beam. While a BEC in its ground state simply leads to isotropic emission, vortices embedded in the condensate will create higher angular-momentum modes in the laser profile. In particular, a BEC bearing a single vortex provides a *p*-wave ballistic tunneling source (Sec. V A). The particle distribution generated by it depends strongly on the relative orientation of vortex and gravitational force: In parallel alignment, the vortex is simply preserved in the profile, while the perpendicular setup features a conspicuous detuning-dependent node structure in the atom distribution. Finally, we also discussed the properties of an atom laser outcoupled from a rapidly rotating BEC sustaining a vortex lattice (Sec. V B). The rotating beam wave function thus created is a coherent superposition of ballistic multipole waves with various angular momenta, and the resulting laser profile starkly depends on the detuning from resonance, while the total outcoupling rate shows little variation.

ACKNOWLEDGMENTS

We appreciate helpful discussions with C. Blondel. C.B. would like to thank the Alexander-von-Humboldt Foundation and the Killam Trust for financial support. T.K. received a research grant from the Leonhard–Lorenz-Stiftung. This work was partially funded through the DFG Project No. Kl315/6-1.

APPENDIX A: TRANSLATION THEOREM FOR HARMONIC POLYNOMIALS

In this appendix, we present a formula that allows to expand a harmonic polynomial $K_{lm}(\mathbf{r}+\mathbf{a})$ with shifted center into a spherical power series with respect to the origin, i.e., in the variable $\mathbf{r}$. Since the position variables $\mathbf{r}$ and $\mathbf{a}$ in the argument are interchangeable, the same series will also furnish the expansion of $K_{lm}(\mathbf{r}+\mathbf{a})$ around $\mathbf{a}$. Hence, we expect the general form for this series

$$K_{lm}(\mathbf{r}+\mathbf{a})=\sum_{\lambda=0}^{l}\sum_{\mu=-\lambda}^{\lambda} C_{\lambda\mu}^{lm}K_{\lambda\mu}(\mathbf{r})K_{l-\lambda,m-\mu}(\mathbf{a}), \tag{A1}$$

where $C_{\lambda\mu}^{lm}=C_{l-\lambda,m-\mu}^{lm}$ must hold. (Note that $K_{lm}(\mathbf{r})$ is a homogeneous polynomial of order l, so the orders in the right-hand side products of harmonic polynomials in Eq. (A1) must add up to l. Similarly, the sum of their magnetic quantum numbers must be m.) The coefficients $C_{\lambda\mu}^{lm}$ in Eq. (A1) have been determined in Refs. [23,68,69]:

$$C_{\lambda\mu}^{lm}=\sqrt{\frac{4\pi(2l+1)}{(2\lambda+1)(2l-2\lambda+1)}\binom{l+m}{\lambda+\mu}\binom{l-m}{\lambda-\mu}}. \tag{A2}$$

In particular, $C_{00}^{lm}=\sqrt{4\pi}$. (For $|m-\mu|>l-\lambda$, the coefficient vanishes.)

The general series (A1) simplifies if the shift in the argument of $K_{lm}(\mathbf{r}+\mathbf{a})$ takes place along the axis of quantization, i.e., $\mathbf{a}=a\hat{\boldsymbol{e}}_z$. Then, rotational symmetry around the z axis is preserved, and the quantum number m is unaffected by the translation. Hence, only terms with $\mu=m$ survive in Eq. (A1). Inserting the explicit value $K_{\lambda 0}(a\hat{\boldsymbol{e}}_z)=\sqrt{(2\lambda+1)/4\pi}a^{\lambda}$ [13], we obtain [17,18]

$$K_{lm}(\mathbf{r}+a\hat{\boldsymbol{e}}_z)=\sum_{j=|m|}^{l} T_{jlm}a^{l-j}K_{jm}(\mathbf{r}), \tag{A3}$$

where the translation coefficient T_{jlm} is given by Eq. (A2):

$$T_{jlm}=\sqrt{\frac{2l+1}{2j+1}\binom{l+m}{j+m}\binom{l-m}{j-m}}. \tag{A4}$$

APPENDIX B: SOME INTEGRALS INVOLVING AIRY FUNCTIONS

1. The functions $Q_k(\rho,\zeta;\epsilon)$

In the course of our investigation into ballistic multipole matter waves, integral expressions of the type

$$Q_k(\rho,\zeta;\epsilon)=\frac{i}{2\pi\sqrt{\pi}}\int_0^{\infty}\frac{d\tau}{(i\tau)^{k+1/2}}\exp\left\{i\left[\frac{\rho^2}{\tau}+\tau(\zeta-\epsilon)-\frac{\tau^3}{12}\right]\right\} \tag{B1}$$

are frequently encountered. For integer indices k, this set of integrals permits explicit evaluation in terms of products of Airy functions. Introducing the Airy Hankel function $\mathrm{Ci}(u)=\mathrm{Bi}(u)+i\mathrm{Ai}(u)$ [34], the basic member of this class reads

$$Q_0(\rho,\zeta;\epsilon)=\mathrm{Ai}(\epsilon-\zeta+\rho)\mathrm{Ci}(\epsilon-\zeta-\rho). \tag{B2}$$

(A proof of this identity using physical arguments is found in Ref. [5].) From the definition (B1), two recurrence formulas for increasing and decreasing value of the index k are immediately available:

$$Q_{k+1}(\rho,\zeta;\epsilon)=-\frac{1}{2\rho}\frac{\partial}{\partial\rho}Q_k(\rho,\zeta;\epsilon), \tag{B3}$$

$$Q_{k-1}(\rho,\zeta;\epsilon)=\frac{\partial}{\partial\zeta}Q_k(\rho,\zeta;\epsilon). \tag{B4}$$

From a practical point of view, the expressions thus obtained become rather unwieldy with growing $|k|$. The following five-point recursion relation, again easily verified using the integral representation (B1), presents a favorable alternative:

$$\rho^2 Q_{k+2}(\rho,\zeta;\epsilon)-\left(k+\frac{1}{2}\right)Q_{k+1}(\rho,\zeta;\epsilon)+(\zeta-\epsilon)Q_k(\rho,\zeta;\epsilon)+\frac{1}{4}Q_{k-2}(\rho,\zeta;\epsilon)=0. \tag{B5}$$

Finally, we inquire into the asymptotic behavior of Eq. (B1) in the limit $\rho\to 0$. For $k\geqslant 1$, small values of τ provide the bulk contribution to the integral, which allows us to neglect the linear and cubic terms in the exponent of Eq. (B1). In this approximation, the integral evaluates to a Γ function of half-integer argument [34]:

$$Q_k(\rho,\zeta;\epsilon)\sim\frac{\Gamma(k-1/2)}{2\pi^{3/2}\rho^{2k-1}}=\frac{(2k-3)!!}{2^k\pi\rho^{2k-1}}. \tag{B6}$$

The divergence for $\rho\to 0$, however, affects only the real part of $Q_k(\rho,\zeta;\epsilon)$.

2. The functions $\mathrm{Qi}_k(\epsilon)$

Another important class of functions that regularly appears when calculating ballistic total currents is contained in Eq. (B1) as a limiting case

$$\mathrm{Qi}_k(\epsilon)=\lim_{\rho\to 0}\lim_{\zeta\to 0}\mathrm{Im}\{Q_k(\rho,\zeta;\epsilon)\}. \tag{B7}$$

Unlike the functions $Q_k(\rho,\zeta;\epsilon)$ that are divergent in this limit for $k>0$ (reflecting the multipole source singularity), their imaginary parts $\mathrm{Qi}_k(\epsilon)$ remain well defined. Obviously, $\mathrm{Qi}_0(\epsilon)=\mathrm{Ai}(\epsilon)^2$, and all other expressions are available from suitably modified recurrences (B3) and (B4):

$$\mathrm{Qi}_k(\epsilon)=\lim_{z\to 0}\left[-\frac{1}{2z}\frac{\partial}{\partial z}\right]^k\mathrm{Ai}(\epsilon+z)\mathrm{Ai}(\epsilon-z), \tag{B8}$$

$$\mathrm{Qi}_{-k}(\epsilon)=\lim_{z\to 0}\frac{\partial^k}{\partial z^k}\mathrm{Ai}(\epsilon-z)^2 \tag{B9}$$

($k\geqslant 0$). Thus, $\mathrm{Ai}(\epsilon+z)\mathrm{Ai}(\epsilon-z)$ and $\mathrm{Ai}(\epsilon-z)^2$ are generating functions for $\mathrm{Qi}_k(\epsilon)$. In practice, we prefer a recursion relation adapted from Eq. (B5),

$$\left(k+\frac{1}{2}\right)\mathrm{Qi}_{k+1}(\epsilon)+\epsilon\,\mathrm{Qi}_k(\epsilon)-\frac{1}{4}\mathrm{Qi}_{k-2}(\epsilon)=0. \tag{B10}$$

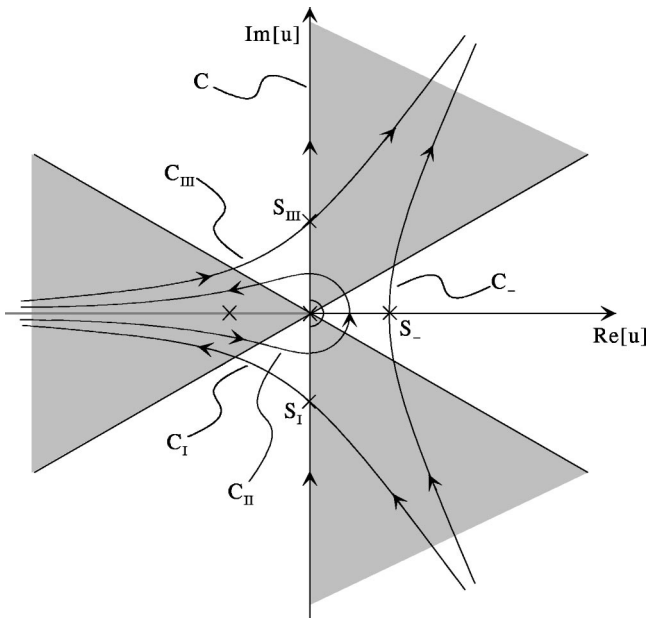

FIG. 8. Evaluation of the integral (B11). The figure displays the original contour C and its shifted counterparts for large values of ϵ. For $\epsilon>0$, the contour is deformed to C_- and runs through the saddle point $S_-=2\sqrt{\epsilon}$. In the case $\epsilon<0$, the contour is split into three parts C_I, C_II, C_III that traverse the saddle points S_I, S_III at $\pm 2i\sqrt{\epsilon}$, but avoid the cut in the complex u plane (gray) by circling the singularity at $u=0$. The integrand asymptotically vanishes in the shaded sectors.

Next, we aim to establish the asymptotic behavior of the functions $\mathrm{Qi}_k(\epsilon)$ in the limit $|\epsilon|\to\infty$. We observe that the integral representation of these functions in Eqs. (B1) and (B7) may be rewritten as a complex contour integral

$$\mathrm{Qi}_k(\epsilon)=\frac{1}{4i\pi\sqrt{\pi}}\int_C\frac{du}{u^{k+1/2}}e^{-\epsilon u+u^3/12}. \tag{B11}$$

Here, the paths C leads along the imaginary axis, avoiding the singularity at the origin and the cut in the complex plane which we choose to place onto the negative real axis (see Fig. 8).

For large values of $|\epsilon|$, a saddle-point approximation for Eq. (B11) is in order. This poses no problems for $\epsilon\to+\infty$ (tunneling case). Then, the relevant stationary point of the exponent $S_-=2\sqrt{\epsilon}$ is readily identified, and shifting the path of integration (see Fig. 8) ultimately yields the asymptotic series,

$$\mathrm{Qi}_k(\epsilon)\sim\frac{1}{2\pi}(2\sqrt{\epsilon})^{-(k+1)}\exp\left(-\frac{4}{3}\epsilon^{3/2}\right)\left[1-\frac{3k^2+9k+5}{24\epsilon^{3/2}}+O\left(\frac{1}{\epsilon^3}\right)\right]. \tag{B12}$$

The situation is more involved for $\epsilon\to-\infty$ (classically allowed motion). Here, the saddle points are located at $S_{\mathrm{I,III}}$

$=\mp 2i\sqrt{|\epsilon|}$, and the direction of steepest descent cuts the imaginary axis under an angle of $\pi/4$. Hence, the integration path must be deformed to lead into the sector of asymptotically vanishing integrand $|\arg u|>5\pi/6$. Due to the presence of the cut in the complex plane, the partial paths C_{I}, C_{III} cannot be simply connected as $\mathrm{Re}[u]\to-\infty$, but must be linked by an additional path element C_{II} that loops back around the singularity located at $u=0$, as indicated in Fig. 8. The latter contribution is asymptotically evaluated by means of Hankel's integral formula [70] that states $\int_{C_{\mathrm{II}}} e^t t^{-z} dt = 2\pi i/\Gamma(z)$:

$$\int_{C_{\mathrm{II}}} \frac{du}{u^{k+1/2}} e^{-\epsilon u+u^3/12} \sim 2\pi i \frac{|\epsilon|^{k-1/2}}{\Gamma(k+1/2)}. \qquad \text{(B13)}$$

This secular part thus obeys a simple power-law dependence reminiscent of the Wigner law (25), while the saddle points S_{I}, S_{III} contribute conjugate complex oscillatory terms similar in structure to Eq. (B12):

$$\int_{C_{\mathrm{III}}} \frac{du}{u^{k+1/2}} e^{-\epsilon u+u^3/12} \sim \frac{2i\sqrt{\pi}\exp\left(\frac{4i}{3}|\epsilon|^{3/2}\right)}{(2i\sqrt{|\epsilon|})^{k+1}}. \qquad \text{(B14)}$$

Rearranging Eqs. (B13) and (B14), the leading asymptotic form for $\mathrm{Qi}_k(\epsilon)$ as $\epsilon\to-\infty$ follows:

$$\mathrm{Qi}_k(\epsilon) \sim \frac{1}{2\sqrt{\pi}} \frac{|\epsilon|^{k-1/2}}{\Gamma(k+1/2)} + \frac{\sin\left(\frac{4}{3}|\epsilon|^{3/2}-\frac{k\pi}{2}\right)}{2\pi(2\sqrt{|\epsilon|})^{k+1}}. \qquad \text{(B15)}$$

[1] J. Schwinger, *Particles, Sources, and Fields* (Addison-Wesley, Reading, 1973), Vol. 2.
[2] C. Bracher, M. Riza, and M. Kleber, Phys. Rev. B **56**, 7704 (1997).
[3] T. Kramer, C. Bracher, and M. Kleber, Europhys. Lett. **56**, 471 (2001).
[4] T. Kramer, C. Bracher, and M. Kleber, J. Phys. A **35**, 8361 (2002).
[5] C. Bracher, W. Becker, S. Gurvitz, M. Kleber, and M. Marinov, Am. J. Phys. **66**, 38 (1998).
[6] C. Blondel, C. Delsart, and F. Dulieu, Phys. Rev. Lett. **77**, 3755 (1996).
[7] C. Blondel, C. Delsart, F. Dulieu, and C. Valli, Eur. Phys. J. D **5**, 207 (1999).
[8] M.-O. Mewes, M. Andrews, D. Kurn, D. Durfee, C. Townsend, and W. Ketterle, Phys. Rev. Lett. **78**, 582 (1997).
[9] I. Bloch, T. Hänsch, and T. Esslinger, Phys. Rev. Lett. **82**, 3008 (1999).
[10] K. Madison, F. Chevy, W. Wohlleben, and J. Dalibard, Phys. Rev. Lett. **84**, 806 (2000).
[11] J. Abo-Shaeer, C. Raman, J. Vogels, and W. Ketterle, Science **292**, 476 (2001).
[12] P. Engels, I. Coddington, P.C. Haljan, and E.A. Cornell, Phys. Rev. Lett. **89**, 100403 (2002).
[13] A. Messiah, *Quantum Mechanics* (North-Holland, Amsterdam, 1964), Vol. 1.
[14] E. Economou, *Green's Functions in Quantum Physics*, Solid-State Sciences Vol. 7 (Springer, Berlin, 1983).
[15] I. Halperin and L. Schwartz, *Introduction to the Theory of Distributions* (University of Toronto Press, Toronto, 1952).
[16] J. Tersoff and D. Hamann, Phys. Rev. Lett. **50**, 1998 (1983).
[17] E. Hobson, *The Theory of Spherical and Ellipsoidal Harmonics* (Cambridge University Press, Cambridge, 1931).
[18] P. Morse and H. Feshbach, *Methods of Theoretical Physics* (McGraw-Hill, New York, 1953), Vol. 2.
[19] C. Müller, *Spherical Harmonics*, Lecture Notes in Mathematics Vol. 17 (Springer, Berlin, 1966).
[20] B. Bayman, J. Math. Phys. **19**, 2558 (1978).
[21] E. Rowe, J. Math. Phys. **19**, 1962 (1978).
[22] E. Weniger and E. Steinborn, J. Math. Phys. **24**, 2553 (1983).
[23] C. Bracher, Ph.D. thesis, Technische Universität München, 1999.
[24] E. Wigner, Phys. Rev. **73**, 1002 (1948).
[25] L. Hostler, J. Math. Phys. **5**, 591 (1963).
[26] L. Hostler and R. Pratt, Phys. Rev. Lett. **10**, 469 (1964).
[27] V. Bakhrakh and S. Vetchinkin, Teor. Mat. Fiz. **6**, 392 (1971) [Theor. Math. Phys. **6**, 283 (1971)].
[28] G. Gountaroulis, Phys. Lett. **40A**, 132 (1972).
[29] V. Dodonov, I. Malkin, and V. Man'ko, Phys. Lett. **51A**, 133 (1975).
[30] I. Fabrikant, Phys. Rev. A **43**, 258 (1991).
[31] F. Dalidchik and V. Slonim, Zh. Éksp. Teor. Fiz. **70**, 47 (1976) [Sov. Phys. JETP **43**, 25 (1976)].
[32] Y. Li, C. Liu, and S. Franke, J. Acoust. Soc. Am. **87**, 2285 (1990).
[33] B. Gottlieb, M. Kleber, and J. Krause, Z. Phys. A: Hadrons Nucl. **339**, 201 (1991).
[34] *Handbook of Mathematical Functions*, edited by M. Abramowitz and I. Stegun (Dover, New York, 1965).
[35] I. Fabrikant, Zh. Éksp. Teor. Fiz. **79**, 2070 (1980) [Sov. Phys. JETP **52**, 1045 (1981)].
[36] Y. Demkov, V. Kondratovich, and V. Ostrovskii, Pis'ma Zh. Éksp. Teor. Fiz. **34**, 425 (1981) [JETP Lett. **34**, 403 (1982)].
[37] M. Du, Phys. Rev. A **40**, 4983 (1989).
[38] V. Kondratovich and V. Ostrovskii, J. Phys. B **23**, 3785 (1990).
[39] G. Möllenstedt and C. Jönsson, Z. Phys. **155**, 472 (1959).
[40] R. Feynman and A. Hibbs, *Quantum Mechanics and Path Integrals* (McGraw-Hill, New York, 1965).
[41] L. Schulman, *Techniques and Applications of Path Integration* (Wiley, New York, 1981).
[42] S. Horch and R. Morin, J. Appl. Phys. **74**, 3652 (1993).
[43] N. Manakov, M. Frolov, A. Starace, and I. Fabrikant, J. Phys. B **33**, R141 (2000).
[44] M. Du and J. Delos, Phys. Lett. A **134**, 476 (1989).
[45] I. Fabrikant, Zh. Éksp. Teor. Fiz. **83**, 1675 (1982) [Sov. Phys. JETP **56**, 967 (1982)].

[46] H. Wong, A. Rau, and C. Greene, Phys. Rev. A **37**, 2393 (1988).
[47] M. Du and J. Delos, Phys. Rev. A **38**, 5609 (1988).
[48] V. Kondratovich and V. Ostrovskii, J. Phys. B **23**, 21 (1990).
[49] I. Fabrikant, J. Phys. B **27**, 4545 (1994).
[50] P. Golovinskii, Zh. Éksp. Teor. Fiz. **112**, 1574 (1997) [Sov. Phys. JETP **85**, 857 (1997)].
[51] H. Bryant *et al.*, Phys. Rev. Lett. **58**, 2412 (1987).
[52] N. Gibson, B. Davies, and D. Larson, Phys. Rev. A **47**, 1946 (1993).
[53] N. Gibson, B. Davies, and D. Larson, Phys. Rev. A **48**, 310 (1993).
[54] N. Gibson, M. Gasda, K. Moore, D. Zawistowski, and C. Walter, Phys. Rev. A **64**, 061403 (2001).
[55] C. Nicole, H. Offerhaus, M. Vrakking, F. Lépine, and C. Bordas, Phys. Rev. Lett. **88**, 133001 (2002).
[56] *Atoms in Intense Fields*, edited by M. Gavrila, Advances in Atomic, Molecular, and Optical Physics, Supplement Vol. 1 (Academic Press, London, 1992).
[57] A. Lohr, M. Kleber, R. Kopold, and W. Becker, Phys. Rev. A **55**, R4003 (1997).
[58] E. Luc-Koenig and A. Bachelier, J. Phys. B **13**, 1769 (1980).
[59] V. Slonim and F. Dalidchik, Zh. Éksp. Teor. Fiz. **71**, 2057 (1976) [Sov. Phys. JETP **44**, 1081 (1976)].
[60] A. Chikkatur, Y. Shin, A. Leanhardt, D. Kielpinski, E. Tsikata, T. Gustavson, D. Pritchard, and W. Ketterle, Science **296**, 2193 (2002).
[61] A. Fetter and A. Svidzinsky, J. Phys.: Condens. Matter **13**, R135 (2001).
[62] P. Haljan, B. Anderson, I. Coddington, and E. Cornell, Phys. Rev. Lett. **86**, 2922 (2001).
[63] Y. Japha and B. Segev, Phys. Rev. A **65**, 063411 (2002).
[64] A. Edmonds, *Angular Momentum in Quantum Mechanics* (Princeton University Press, Princeton, 1957).
[65] M. Matthews, B. Anderson, P. Haljan, D. Hall, C. Wieman, and E. Cornell, Phys. Rev. Lett. **83**, 2498 (1999).
[66] D. Butts and D. Rokhsar, Nature (London) **397**, 327 (1999).
[67] T.-L. Ho, Phys. Rev. Lett. **87**, 060403 (2001).
[68] M. Caola, J. Phys. A **11**, L23 (1978).
[69] S. Chakrabarti and D. Dewangan, J. Phys. B **28**, L769 (1995).
[70] F. Olver, *Asymptotics and Special Functions* (Academic Press, New York, 1974).